7 Cardiovascular Magnetic Resonance Imaging

Warren J. Manning

Key Points

- Spin-echo imaging is commonly used for assessment of cardiac and great vessel anatomy. With classic spin-echo imaging, rapidly moving blood appears dark.
- At current field strengths (1.5 and 3.0 tesla), cardiovascular magnetic resonance (CMR) imaging is considered safe for bioprosthetic and mechanical heart valves.
- Older (pre-2000) cardiac pacemakers and implantable defibrillators are an absolute contraindication to higher field (≥0.5 T) CMR. Patients with newer pacemaker systems may be safely scanned using specific protocols.
- Cardiovascular magnetic resonance is an important noninvasive technique for evaluating thoracic aortic aneurysms.
- The clinical "gold standard" for the diagnosis of pulmonary embolism is contrast CT angiography (CTA). For patients who are not candidates for CTA due to renal dysfunction or contrast allergic history, pulmonary artery magnetic resonance angiography (MRA) is an excellent noninvasive alternative with high sensitivity and specificity.
- Cine CMR provides an excellent means for quantitative assessment of left and right ventricular volumes, global ejection fraction, regional systolic function, and biventricular mass.
- Available data suggest dobutamine stress CMR is a sensitive technique for the noninvasive recognition of coronary artery disease (CAD).
- Coronary artery bypass graft patency is well evaluated by spin echo, gradient echo, and gadolinium–diethylenetriamine pentaacetic acid (DTPA)-enhanced three-dimensional (3D) enhanced coronary magnetic resonance imaging (MRI).
- Cardiovascular magnetic resonance provides the noninvasive means to assess myocardial viability and fibrosis accurately.
- Cardiovascular magnetic resonance has great value for characterizing paracardiac and extracardiac tumors and their extension into the myocardium, cardiac chambers, or neighboring mediastinal structures.
- Both spin-echo CMR and CT are capable of measuring pericardial thickness accurately.
- Cardiovascular magnetic resonance has great utility for both simple and complex congenital heart disease. Coronary MRI for identification and characterization of anomalous coronary arteries is widely accepted.

More than any other noninvasive imaging technique, the flexibility of cardiovascular magnetic resonance (CMR) imaging offers the promise to dramatically expand our ability to evaluate patients with known or suspected cardiovascular disease. The combined attributes of superior image quality and flexibility for assessment of cardiac anatomy, ventricular function, viability, perfusion, valvular function, great vessel anatomy, blood flow, and native coronary artery and coronary artery bypass graft integrity give CMR unmatched potential for the comprehensive evaluation of the cardiovascular system. Currently accepted clinical applications of CMR continue to expand rapidly[1] (Table 7.1). Hardware (gradients and high field systems) advances now allow for sub-second data acquisitions with "real-time" imaging, and software advances and novel contrast agents promise to further exploit CMR's advantages over competing noninvasive imaging methods. The introduction of a comprehensive CMR examination,[2,3] in which cardiac anatomy, function, viability, perfusion, valvular, and coronary artery assessment is performed

TABLE 7.1. Current clinical applications for cardiovascular magnetic resonance (CMR)

1. Indications for CMR in acquired diseases of the vessels
   a. Diagnosis and monitoring of thoracic aortic aneurysm, dissection, aortic wall hematoma, and penetrating ulcer
   b. Assessment of pulmonary artery dilation and dissection
   c. Characterization of pulmonary vein stenosis
2. Indications for CMR in coronary artery disease
   a. Assessment of global and regional left and right ventricular systolic function at rest and with pharmacologic stress
   b. Assessment of regional myocardial perfusion at rest and stress
   c. Determination of viability
3. Indications for CMR in valvular heart disease
   a. Assessment of the severity of aortic stenosis and mitral stenosis
   b. Quantitative assessment of mitral and aortic regurgitation
4. Indications for CMR in cardiomyopathies and pericardial disease
   a. Differentiation of ischemic versus nonischemic cardiomyopathy and underlying etiology (including hypertrophic cardiomyopathy, noncompaction, arrhythmic right ventricular cardiomyopathy (ARVC), and iron deposition)
   b. Characterization of mass, biventricular volumes, and ejection fraction
   c. Identification of pericardial thickening, circumferential, and local pericardial effusions
5. Indications for CMR in congenital heart disease
   a. Anomalous coronary artery disease
   b. Quantification of intracardiac shunt
   c. Characterization of simple and complex coronary anatomy
   d. Identification of aortic and pulmonary pathology (e.g., coarctation, patent ductus arteriosus)
   e. Characterization of anomalies of the ventricles
   f. Anomalous pulmonary venous drainage

Adapted from Pennell et al.[1]

during a single 1-hour session, will lead to decreased utilization of other imaging tests (e.g., echocardiography, radionuclide ventriculography and radionuclide perfusion, diagnostic x-ray coronary angiography), especially for follow-up care/monitoring. Cardiovascular magnetic resonance training guidelines for both those in fellowship[4,5] and practitioners who have completed fellowship have now been developed.[5–7] The relative cost advantage/disadvantage of CMR as compared with these other imaging technologies will need to be defined by future cost-effectiveness studies.

Technical Considerations

A review of magnetic resonance (MR) physics is beyond the scope of this chapter, and readers are referred elsewhere.[8,9] Unlike other imaging techniques, CMR images may depict blood and other tissues as bright, dark, or of an intermediate intensity depending on the specific CMR sequence that is employed, the use of exogenous contrast, and whether the tissue of interest (e.g., blood) is rapidly or slowly moving, and whether blood flow is laminar or turbulent. The most common CMR approaches are the spin echo ("black blood"), the k-space segmented gradient echo, and the steady-state free precession (SSFP; trueFISP, balanced FFE, FIESTA; "bright blood") sequences.

Spin-echo imaging is commonly used for assessment of cardiac and great vessel anatomy. With classic spin-echo imaging, rapidly moving blood appears dark because a pair (90 and 180 degrees) of sequential radiofrequency (RF) pulses is applied. Rapidly moving blood will move out of the imaging plane during the time interval between these two RF pulses, leading to an absence of signal, or flow void (i.e., "black blood"). Stagnant blood, which would be exposed to both RF pulses, will appear relatively bright. Variations may be highlighted when viewing an image containing blood experiencing different phases of the cardiac cycle (e.g., early systole, where there may be rapid flow in the ascending aorta with relatively stationary flow in the descending thoracic aorta). The flow void can be emphasized using thin sections or longer echo times.

With gradient-echo sequences, commonly used for function/cine CMR, a single RF pulse is applied with a much shorter echo time. Little signal is then lost due to washout effects, but stationary tissue (often surrounding blood vessels; e.g., muscle) will be saturated because of repeated RF stimulation. Thus, signal from stationary tissues is suppressed ("dark") due to repeated RF stimulation, while areas of rapid blood flow (arterial flow) will have continuous inflow of unsaturated blood with a resultant "bright" signal. Therefore, on gradient-echo images, rapidly moving laminar blood flow appears bright, while stagnant blood will appear relatively "dark." In addition, areas of turbulent/chaotic blood flow (corresponding to valvular stenoses, aortic insufficiency, mitral regurgitation) will appear dark due to local turbulence/phase dispersion. The relative "size" of these signal voids is dependent on the echo time. Steady-state free precession imaging is relatively insensitive to inflow effects and also depicts blood as bright.

Both gradient-echo and SSFP imaging are commonly used for cine CMR imaging of ventricular and valvular function. For all CMR imaging sequences, specific prepulses may highlight or suppress specific tissues (e.g., fat saturation prepulse will suppress signal from fat; inversion recovery (180-degree) prepulses will emphasize T1-weighting). Exogenous intravenous contrast [e.g., gadolinium–diethylenetriamine pentaacetic acid (Gd-DTPA)] may be used in combination with both spin-echo and gradient-echo approaches and has been particularly valuable for viability assessment of myocardial fibrosis/scar, for assessment of regional myocardial perfusion, and for characterization of tumors/masses.[10] These extracellular CMR contrast agents are minimally nephrotoxic with a highly favorable anaphylaxis profile.[11,11a]

Another very useful CMR sequence is phase velocity mapping, in which the velocity of blood perpendicular to the imaging plane is encoded, providing localized flow data somewhat analogous to pulsed Doppler echocardiography. This approach is particularly valuable for quantifying regurgitant volumes and flows through the great vessels, conduits, and valves.

In contrast to general magnetic resonance applications outside of the heart, the vast majority of CMR applications depend on accurate R wave detection for electrocardiographic (ECG) triggering. In the presence of a rate-controlled irregularly irregular rhythm such as atrial fibrillation, image quality will be acceptable,[12] but high-grade ventricular ectopy or a regularly irregular rhythm (e.g., trigeminy) often leads to significant image degradation. In these situations, real-time CMR is often used, with reduction in spatial and temporal resolution.[13] In limited situations, peripheral pulse (PPU) triggering may be adequate, but we have generally found image quality to be inferior to ECG triggering.

Specific Considerations of Cardiovascular Magnetic Resonance in the Cardiac Patient

In addition to general restrictions regarding CMR [ferromagnetic intracranial clips, transcutaneous electrical nerve stimulation (TENS) units, intraauricular implants, shrapnel, etc.], there are also special considerations for CMR (and general magnetic resonance scanning) in the cardiac patient. A comprehensive discussion of CMR safety with regard to implanted devices is beyond the scope of this chapter. Readers are referred to comprehensive sources (www.mrisafety.com).[14] At current field strengths [1.5 and 3.0 tesla (T)], CMR imaging is considered safe for both bioprosthetic and mechanical heart valves.[14] However, a local image artifact (loss of signal/image distortion) will occur in the region immediately surrounding the valve prosthesis (Fig. 7.1). Similarly, sternotomy wires, thoracic vascular clips, and ostial coronary artery bypass graft markers are not a contraindication to imaging, but localized artifacts will be present (Fig. 7.2), thereby limiting assessment of adjacent structures. The relative size of the image artifact is increased with gradient-echo and SSFP sequences (versus spin-echo sequences). While the composition metal of intracoronary stents will cause a local

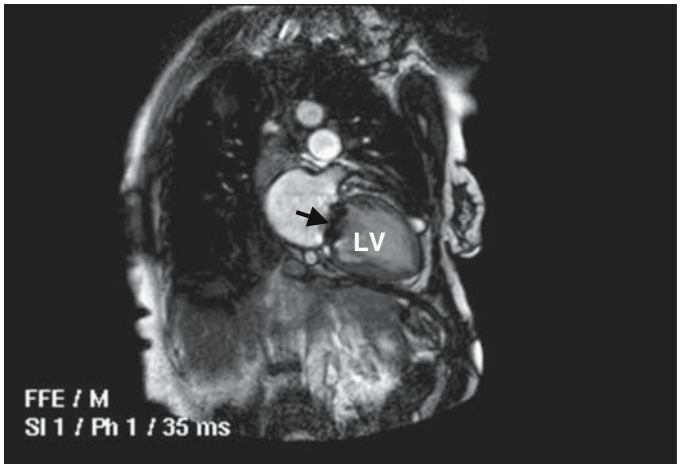

FIGURE 7.1. A single image from a cine cardiovascular magnetic resonance (CMR) in the two-chamber view. Note the artifact (black arrow) resulting from a bileaflet mechanical mitral valve prosthesis. LV, left ventricle.

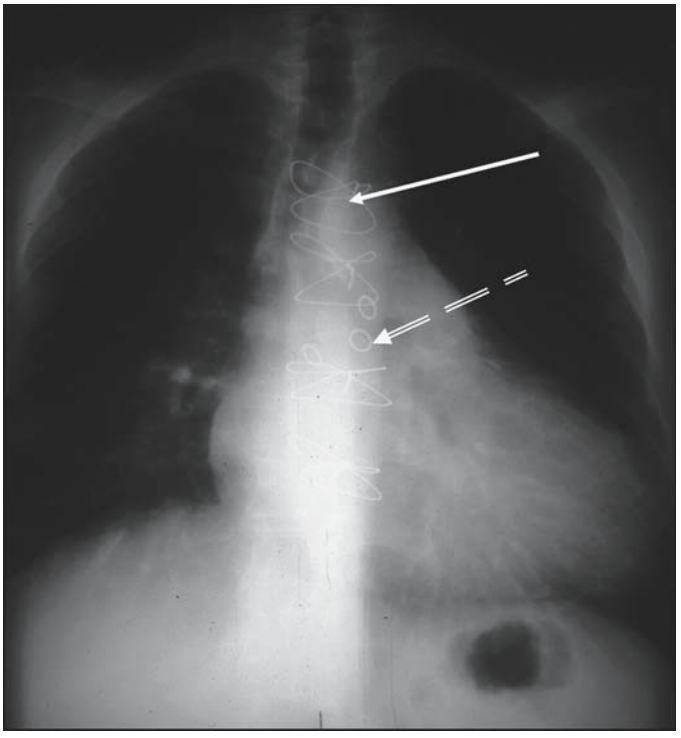

A

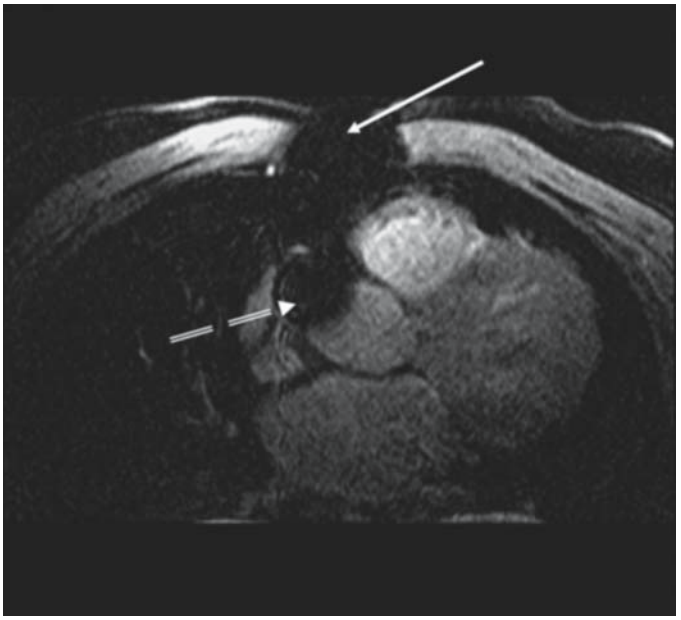

B

FIGURE 7.2. (A) Posteroanterior (PA) chest x-ray in a patient with a prior coronary artery bypass graft surgery with sternal wires (solid arrow) and bypass graft markers (broken arrow). (B) Gradient-echo CMR in the transverse plane at the level of the origin of the saphenous vein bypass grafts. Note the artifacts from the saphenous vein markers (solid arrow) as well as sternal wires (broken arrow).

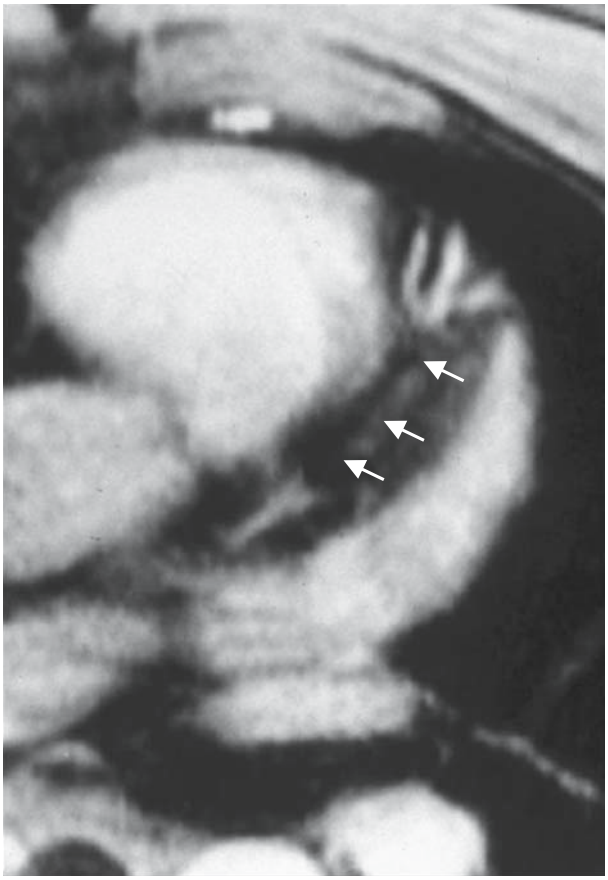

FIGURE 7.3. Gradient-echo coronary CMR in a patient with a widely patent mid-left anterior descending (LAD) stent. Note the signal void in the area corresponding to the stent (white arrows) with visualization of the LAD lumen proximal and distal to the stent.

susceptibility effect (dark area) (Fig. 7.3), no adverse events have been reported at 1.5 T,[15] yet for many years, patients receiving intracoronary stents were instructed to avoid all MR scanning for at least 2 months. This error has now been corrected with the April 2005 decision by the United States Food and Drug Administration (FDA) to approve immediate MR scanning for both the Boston Scientific (Boston, MA) and Johnson & Johnson drug-eluding stents.

The area of safety with regard to CMR scanning among patients with cardiac pacemakers and implantable cardiodefibrillators (ICDs) is currently in a state of flux. When CMR is the only imaging modality available, uncomplicated CMR has been performed at low field strengths (0.2 T) using specific protocols[16] and with proper safeguards in place. Such devices (and the presence of permanent pacemaker leads alone) had been considered an "absolute" contraindication to higher field (≥0.5 T) CMR scanning due to the potential for unpredictable device reprogramming, myocardial stimulation, or heating of the device leads.[14] Protocols have now been described for safe scanning at 1.5 T for patients with modern (post-2000) pacemaker systems.[17,18] This area is likely to receive considerable attention and will evolve in the coming years.

Thoracic Aorta and Great Vessels

For many years, CMR had its greatest clinical impact on the assessment of the thoracic aorta in the patient with known or suspected thoracic aortic aneurysm (Fig. 7.4) or aortic dissection (Fig. 7.5). Cardiovascular magnetic resonance compares favorably to spiral or multidetector computed tomography (CT) because CMR employ no ionizing radiation or requirement for potentially nephrotoxic iodinated contrast. Comprehensive data regarding the presence of a dissection, entry and exit points, the presence of intraluminal thrombus, involvement of the great vessels, and coexistent aortic insufficiency and pericardial effusion are also readily obtained. Transverse, coronal, and sagittal images using ECG gating T1-weighted spin-echo techniques are initially acquired for anatomic imaging.[19,20] The sine qua non of aortic dissection for spin-echo imaging is the identification of an intimal "flap" separating the true and false lumen. Breath-hold 3D contrast-enhanced (CE) magnetic resonance angiogram (MRA) is then obtained to define the aortic lumen either with[21] or without[22,23] ECG gating. Cine SSFP or gradient-echo acquisitions can then be obtained if a dissection flap is identified. In addition to the classic finding of an intimal flap, eccentric aortic wall thickening may also be seen, possibly representing an early dissection or intramural hematoma.[24] In experienced hands, CMR, CT with iodinated contrast, and multiplane transesophageal echocardiography

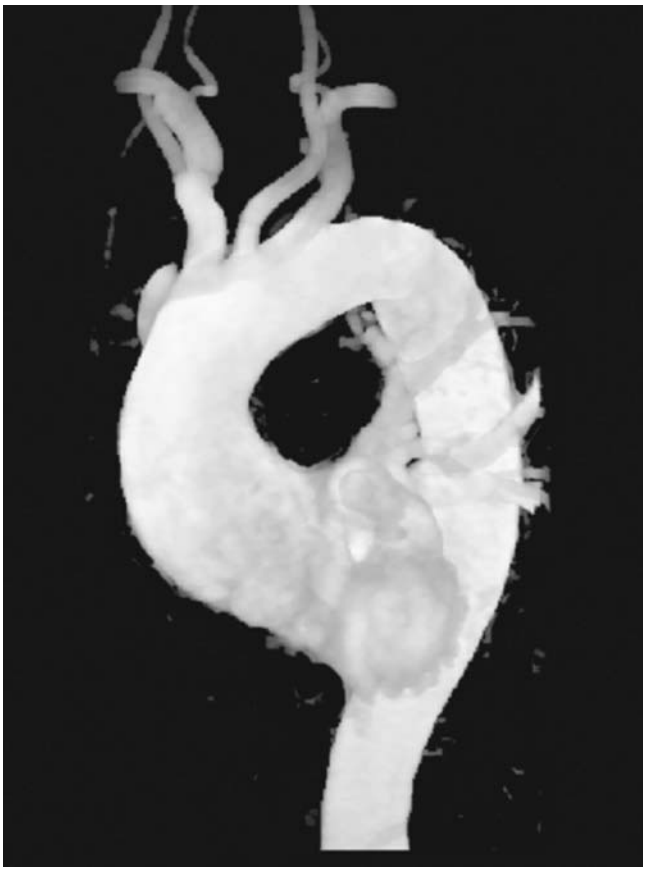

FIGURE 7.4. Aortic aneurysm: three-dimensional (3D) coronary magnetic resonance angiogram (MRA).

(TEE) have similarly high sensitivity, specificity, and accuracy for identification of thoracic aortic dissection.[19,20,25–27] Cardiovascular magnetic resonance and spiral or multidetector CT have specific advantages (as compared with multiplane TEE) for providing information regarding the extent of the dissection into the great vessels and abdominal aorta. Both TEE and CMR also permit determination of aortic valve involvement and aortic insufficiency (Fig. 7.5), though valve morphology is better defined by TEE. Both TEE and CMR can often provide information regarding the involvement of the proximal coronary arteries. Study time and access are important factors in the choice of imaging test. For CMR aortic dissection assessment, a comprehensive assessment can usually be completed within 30 minutes, with close patient monitoring. We generally recommend CMR (or CT) for patients who are hemodynamically stable and for follow-up studies in younger patients with chronic aneurysms or dissection, refer stable older patients with good renal function to CT, and utilize TEE for those with clinical instability, claustrophobia, or renal dysfunction.

In addition to aortic aneurysm and dissection, CMR is also useful for the assessment of congential aortic lesions such as aortic coarctation (Fig. 7.6) and patent ductus arteriosus, as well as more complex abnormalities involving the great vessels (discussed later). Phase velocity methods may be used to quantify velocity gradients[28] as well as flow through shunts and to quantify pulmonic–systemic flows. From a practical perspective, patients with congenital cardiovascular lesions are often referred for CMR imaging for confirmation or better definition of an abnormality identified or suspected on a prior imaging (echocardiography, x-ray angiography) study.

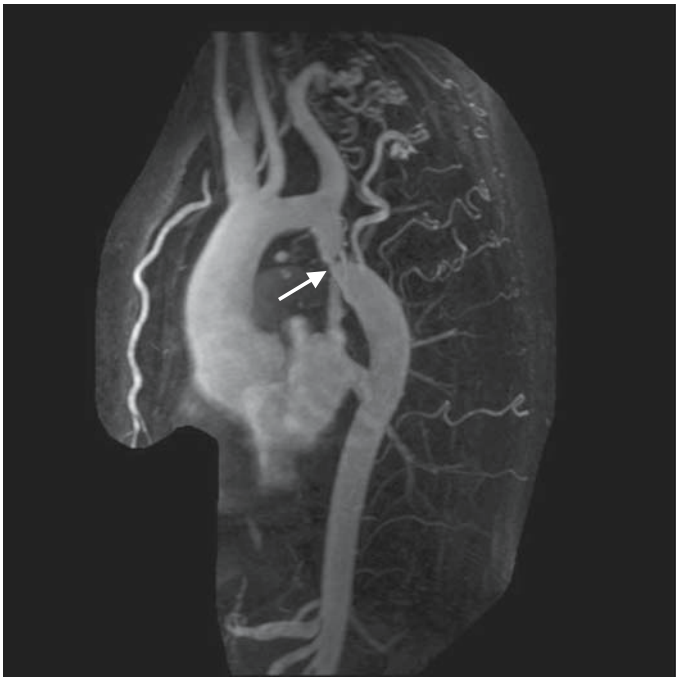

FIGURE 7.6. A 3D contrast-enhanced (CE) magnetic resonance angiogram (MRA) in a 17-year-old boy with an aortic coarctation (arrow). Note the extensive collateral vessels.

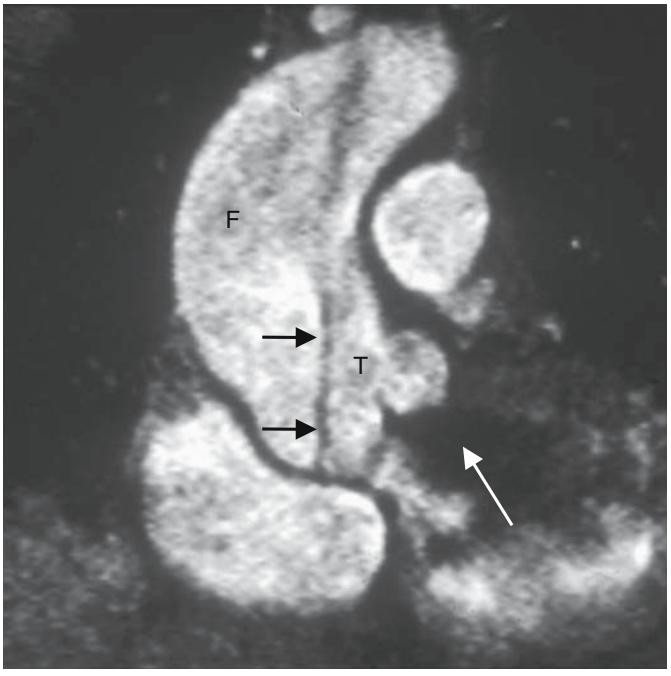

FIGURE 7.5. Coronal diastolic frame cine gradient-echo CMR in a patients with an ascending aortic dissection (black arrows). Note the dissection flap (black arrows) begins immediately superior to the aortic valve leaflet. Flow is seen in both the true (T) and false (F) lumen. Signal void (white arrow) from local turbulence is seen in the left ventricular cavity immediately below the aortic valve and is due to associated aortic insufficiency.

Pulmonary Embolism, Pulmonary Artery, and Pulmonary Vein Assessment

Compared to imaging of the aorta, CMR of the pulmonary artery is more technically demanding of patient cooperation, with breath-holding due to artifacts related to motion as the lungs expand and collapse. Additionally, the pulmonary arteries branch in a complex fashion, with their diameter progressively decreasing at each bifurcation. Finally, susceptibility between the blood–tissue interface and air leads to signal loss at the vessel–lung interface. Although spin-echo approaches can be used to define the anatomy of the pulmonary trunk and the proximal portions of the right and left main pulmonary arteries, 3D CE-MRA is the mainstay of pulmonary artery assessment.[29,30] This is especially applicable to patients who are suspected of having acute (or chronic) pulmonary thromboembolism. The clinical "gold standard" for the diagnosis of pulmonary embolism is contrast x-ray pulmonary angiography and CT angiography (CTA). The latter has become extremely popular with the widespread availability of multidetector CT scanners in the emergency department. For patients who are not candidates for pulmonary CTA due to renal dysfunction or contrast allergic history, pulmonary artery MRA is an excellent noninvasive alternative with high sensitivity and specificity. Similar to conventional angiography, pulmonary emboli present as an abrupt discontinuation (signal void) of the arterial lumen (Fig. 7.7). Pulmonary artery dissection is a rare condition that may mimic aortic dissection in symptoms, for which

FIGURE 7.7. Pulmonary artery 3D CE-MRA in a patient with a pulmonary embolism (arrow) with abrupt loss of vasculature.

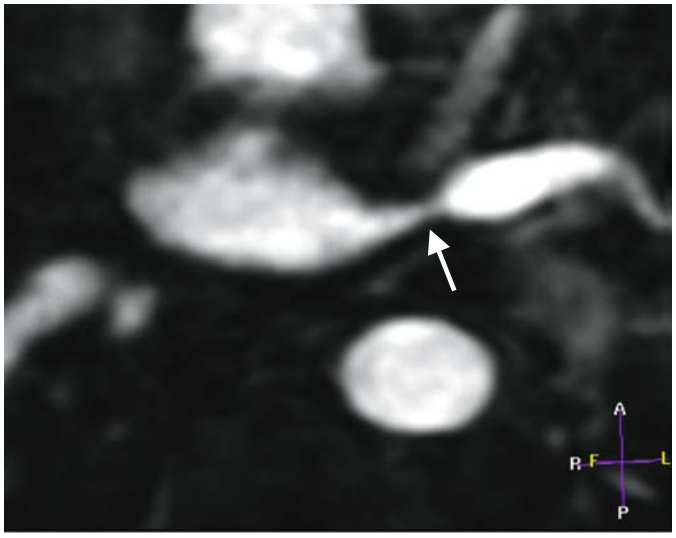

FIGURE 7.8. Pulmonary vein CE-MRA in a 65-year-old man with atrial fibrillation who underwent pulmonary vein ablation 1 month previously. Note the focal stenosis (arrow) of the left lower pulmonary vein.

pulmonary artery CE-MRA as well as gradient-echo and spin-echo methods have been shown to be quite accurate.[31]

With increasing interest in pulmonary vein ablation as a mainstream therapy for patients with atrial fibrillation, monitoring of patients for asymptomatic pulmonary vein stenosis has become important. Pulmonary vein CE-MRA has been shown to be a very accurate method for monitoring the size of the pulmonary arteries[32–34] and for identifying stenoses[32,34,35] (Fig. 7.8). Preliminary data suggest identification of the ablation site is also possible using delayed enhancement CMR methods.[35a]

Quantitative Assessment of Ventricular Volumes and Mass

Although rarely used for first-line assessment, volumetric cine CMR is becoming increasingly recognized as the clinical gold standard for the *quantitative* assessment of left and right ventricular volumes, global ejection fraction, regional systolic function, and biventricular mass (Fig. 7.9) in patients with known disease. Cardiovascular magnetic resonance is used for validation of ventricular volumes assessed by new technologies such as 3D echocardiography and cardiac CT.[36–38] Advantages of CMR include the ability to obtain high temporal and spatial resolution tomographic data in true short- and long-axis orientations, the outstanding endocardial border definition provided by current SSFP sequences, and the relative ease of data analysis. Semiautomated methods allow for the delineation of the endocardial and epicardial borders with very high accuracy and reproducibility for determination of ventricular volumes, stroke volume, and ejection fraction both in normal and focally deformed ventricles.[39–42] As compared with M-mode or 2D echocardiography, which is limited to acoustic windows with suboptimal results in many obese and elderly patients, comprehensive, high temporal and spatial resolution true short-axis volumetric data sets are easily acquired in nearly all subjects in less than 8 minutes. Though in theory 3D echocardiography and cardiac CT offer similar volumetric data, the superior spatial (versus 3D echocardiography) and

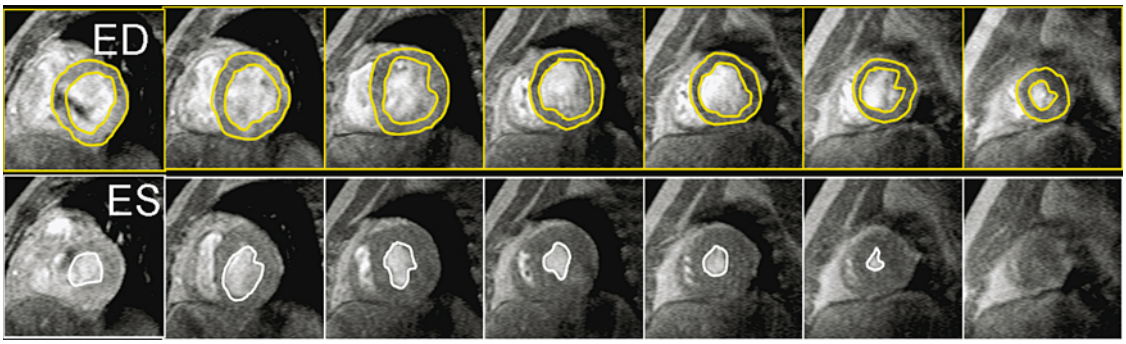

FIGURE 7.9. End-diastolic (ED) and end-systolic (ES) images from cine short-axis data sets demonstrating the use of endocardial border definition and calculation of end-diastolic and end-systolic volumes.

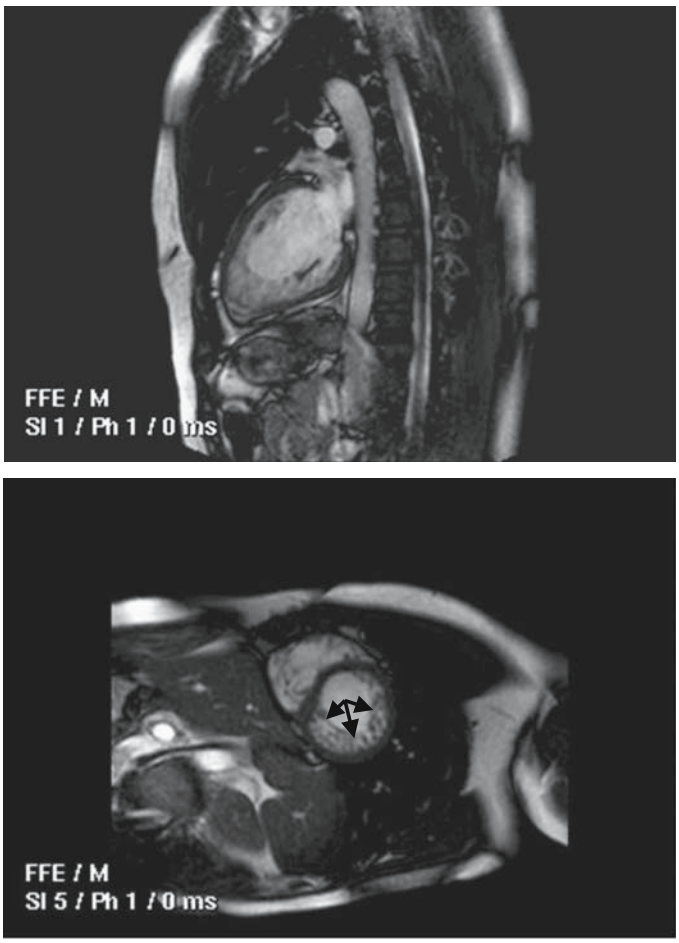

FIGURE 7.10. Cine steady-state free precession (SSFP) images in the (A) two-chamber and (B) short-axis orientations demonstrating prominent trabeculations (arrows) consistent with noncompaction.

temporal (versus CT) resolutions of CMR make it the strong preference when accurate and reproducible assessments are needed. Volumetric CMR is especially valuable for quantitative information regarding left ventricular volume and mass in patients with asymmetric deformations/hypertrophy, and defining cardiomyopathies (such as hypertrophic cardiomyopathy and noncompaction (Fig. 7.10),[43] or monitoring ventricular volumes in patients with regurgitant valvular lesions. Left ventricular aneurysms may be recognized as severe wall thinning (less than 4 mm) and diastolic bulging of the left ventricular free wall (Fig. 7.11). Left ventricular pseudoaneurysm or false aneurysms may also be readily identified on CMR due to their lack of myocardium in the wall of the aneurysm[44] with relatively narrow neck. The superior reproducibility of CMR for both left and right ventricular measures thereby provides more clinical utility in the monitoring

FIGURE 7.11. (A) Cine SSFP two-chamber and delayed enhancement CMR in the (B) two-chamber and (C) short axis orientation of a 54-year-old patient with an inferior infarction and aneurysm. Note the transmural hyperenhancement (B,C) that is visible in the inferior and inferolateral walls with a small thrombus (B, arrow) visible along the subendocardial border.

of patients.[42,45,46] Volumetric CMR methods are also ideal for regional left ventricular assessment with the 17-segment model (six basal, six middle, four apical, with a true apex)[47] that is generally utilized. Left ventricular mural thrombi may be identified on spin-echo images as a density/mass filling the left ventricular apex, especially in an area corresponding to a left ventricular aneurysm[44,48] or as filling defects on cine gradient-echo or SSFP imaging. Delayed enhancement (DE) CMR methods may also depict transmural hyperenhancement in the wall of a true aneurysm with the subendocardial area of hypoenhancement corresponding to a chronic left ventricular thrombus[49,50] (Fig. 7.11). Accurate quantitative evaluation of *right* ventricular volumes, ejection fraction, and mass is also a relatively unique attribute of CMR.[51] For regional assessment of both right and left ventricular systolic function, myocardial tagging techniques have been shown to be more sensitive for quantitation of local dysfunction,[52,53] though their clinical role remains to be defined.

Detection of Coronary Artery Disease

In addition to ventricular volumes and global/regional systolic function, CMR offers several approaches for detecting and evaluating patients with known or suspected coronary artery disease. These include pharmacologic stress testing with β-agonists (regional dysfunction), vasodilators (perfusion deficits), viability imaging, and coronary artery imaging.

Due to distortions of the ECG related to the magnetohydrodynamic of pulsatile blood in the aorta, the ECG is uninterpretable for ischemia within the CMR environment. Thus real-time monitoring of wall motion and close patient supervision is imperative. Physiologic stress is possible within the CMR environment, and supine bicycle ergometry units have been developed for such an application,[54] but pharmacologic stress is more commonly used in combination with graded doses of dobutamine (similar protocols to that used for dobutamine stress echocardiography), with cine images typically acquired in the four- and two-chamber orientations along with three short-axis levels (base, middle, apical) at baseline and at each level of dobutamine (Fig. 7.12). Data suggest that dobutamine stress CMR is more sensitive for the detection of coronary artery disease (versus dobutamine stress echocardiography).[55–57] This superiority is directly related to the enhanced ability of CMR to visualize/define all of the myocardial segments.[50] A study that compared dobutamine CMR stress with vasodilator CMR stress found dobutamine wall motion CMR to be superior (Fig. 7.13).[58] The combination of CMR resting left ventricular ejection fraction and inducible ischemia has prognostic value among patients with known coronary artery disease.[59] Cardiovascular magnetic resonance tagging methods may offer superior sensitivity,[60] but they are less commonly used.

Early applications of CMR myocardial perfusion methods were limited in ventricular coverage, with current methods now acquiring data at three to six short-axis levels during the first passage of Gd-DTPA (0.05 mmol/kg) administered as a tight bolus into the right antecubital fossa. Both visual and quantitative methods (upslope) have been utilized and validated in animal models.[61–63] Comparison studies with x-ray angiography and radionuclide imaging are very good.[64–66] Cardiovascular magnetic resonance protocols of myocardial perfusion may include assessment of perfusion at rest and

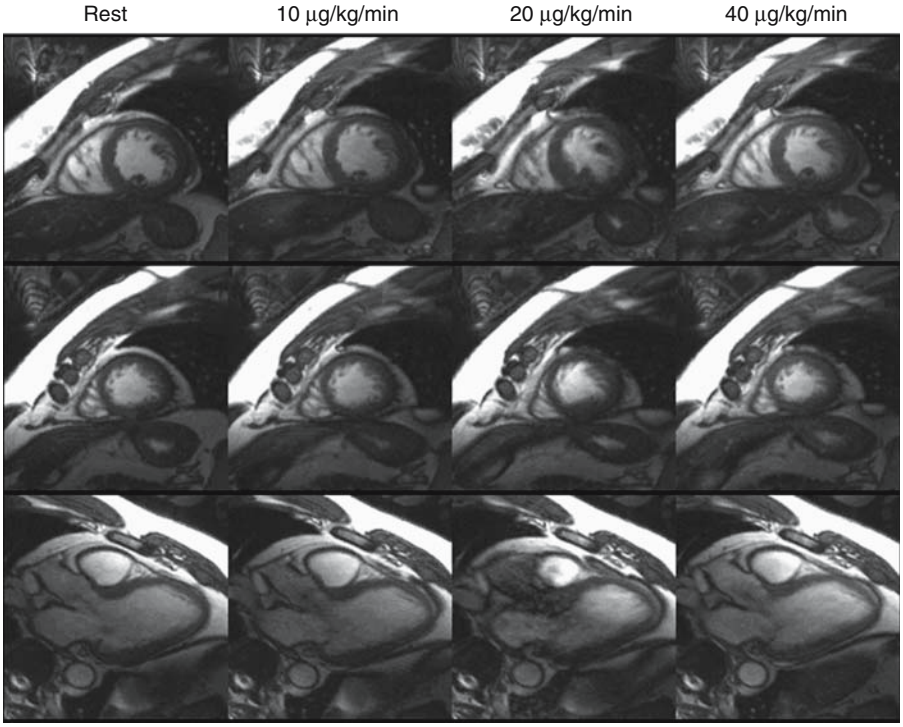

FIGURE 7.12. Common display used for real-time monitoring and subsequent interpretation of dobutamine stress CMR images. Images at rest and gradations of stress are displayed simultaneously for review in the short axis (top two rows) and horizontal long axis (bottom row).

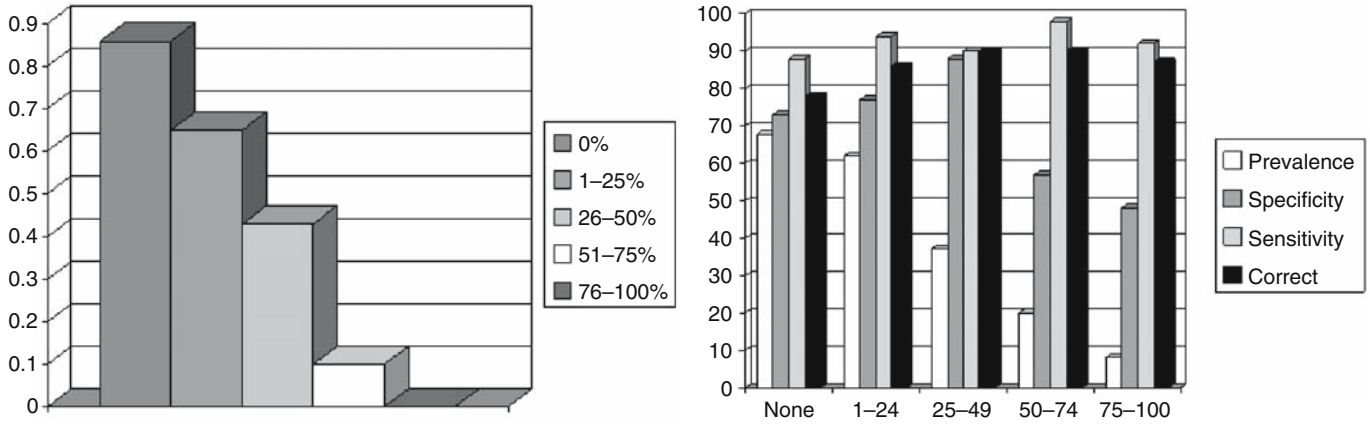

FIGURE 7.13. (A) Likelihood of functional recovery following mechanical revascularization as a function of transmural hyperenhancement with delayed-enhancement (DE)-CMR in patients with regional systolic dysfunction. Dysfunctional regions without any enhancement have a >80% likelihood of functional recovery while those with >50% transmural hyperenhancement have <10% likelihood of recovery. An intermediate finding demonstrates reduced predictive accuracy. (B) Sensitivity, specificity, and accuracy of low-dose dobutamine for prediction of functional recovery after mechanical revascularization appears to be superior to DE-CMR, especially for those with 1% to 49% transmural hyperenhancement.

at peak stress or a single peak-vasodilator assessment with normal resting systolic function used as a surrogate for normal perfusion. Vasodilator perfusion CMR has demonstrated an improvement in myocardial perfusion reserve after a percutaneous coronary intervention[67] and impaired subendocardial perfusion in syndrome X.[68]

Native Coronary Artery Disease Integrity

Cardiovascular magnetic resonance is used routinely for evaluation of vascular beds throughout the body, but coronary MRI is more technically challenging due to the small caliber, tortuosity, and motion related to both the respiratory and cardiac cycle. As a result, CMR assessment of native coronary artery integrity continues to be a field of rapid evolution with recent competition from coronary CTA methods. The relative strengths of coronary MRI include both the lack of substantial ionizing radiation[69] or the need for potentially nephrotoxic/anaphylactic iodinated contrast, or the need to induce bradycardia with beta-blockade. Another disadvantage of coronary CTA is the difficulty with lumen integrity assessment among patients with high risk[70] and older patients due to prominent epicardial calcium.[71] Preliminary data suggest that epicardial calcium does not provide the same interference with coronary MRI depiction of the lumen (Fig. 7.14).[72]

Since the initial descriptions of 2D breath-hold coronary MRI,[73–75] the field has advanced to 3D acquisition methods (double-oblique slab or larger axial stack analogous to coronary CTA) with submillimeter spatial resolution and superior reconstruction capabilities. The spatial resolution of 3D coronary MRI remains inferior to coronary CTA and x-ray coronary angiography, thereby precluding *quantitative* assessments, although the magnitude of the local signal void does correlate with angiographic stenosis.[75] Data acquisition also remains relatively prolonged at 10 to 20 minutes. Despite this limitation, the feasibility of identifying stenoses in the proximal and midcoronary segments has been demonstrated in several single centers.[76,77] At present, some approaches (free breathing navigator with real-time motion correction) remain vendor specific, making multicenter multivendor trials difficult to perform and interpretation of the literature more complicated. We continue to prefer a targeted 3D free-breathing segmented k-space gradient-echo sequence[78,79] using patient specific delay and short acquisition (less than 90 ms/R-R interval) periods.[80] With this approach, high signal intensity (bright blood) represents normal, laminar blood flow, with low signal (signal void) at sites of stenosis and focal turbulence (Fig. 7.15). Despite superior spatial resolution of multidetector CT, a head-to-head comparison of 3D coronary MRI with 16-slice multidetector (using quantitative x-ray coronary angiography as the gold standard) showed similar diagnostic accuracy,[81] including sensitivity and specificity of 75% and 77% for coronary MRI and 82% and 79% for coronary CTA, respectively. A multicenter trial of over 100 patients from seven international sites demonstrated high sensitivity but only modest specificity for identifying focal stenoses, with very high accuracy for discriminating between patients with multivessel disease and no disease.[82] For this reason, we offer coronary MRI as a clinical option for patients presenting with a dilated cardiomyopathy in the absence of a history of acute infarction. Preliminary data from a group of patients with depressed left ventricular systolic function[83] suggest that coronary MRI is superior to DE-CMR for discriminating between these two subsets. Targeted 3D approaches using SSFP methods[84] or a "whole heart" SSFP methodology that supports extensive reconstructions (Fig. 7.16),[85,86] somewhat analogous to multidetector computed tomography (MDCT) acquisitions (though inferior in spatial resolution), have been advocated. Comparative data suggest longer vessel segments have been identified, with improved signal-to-noise ratio (SNR) and contrast-to-noise

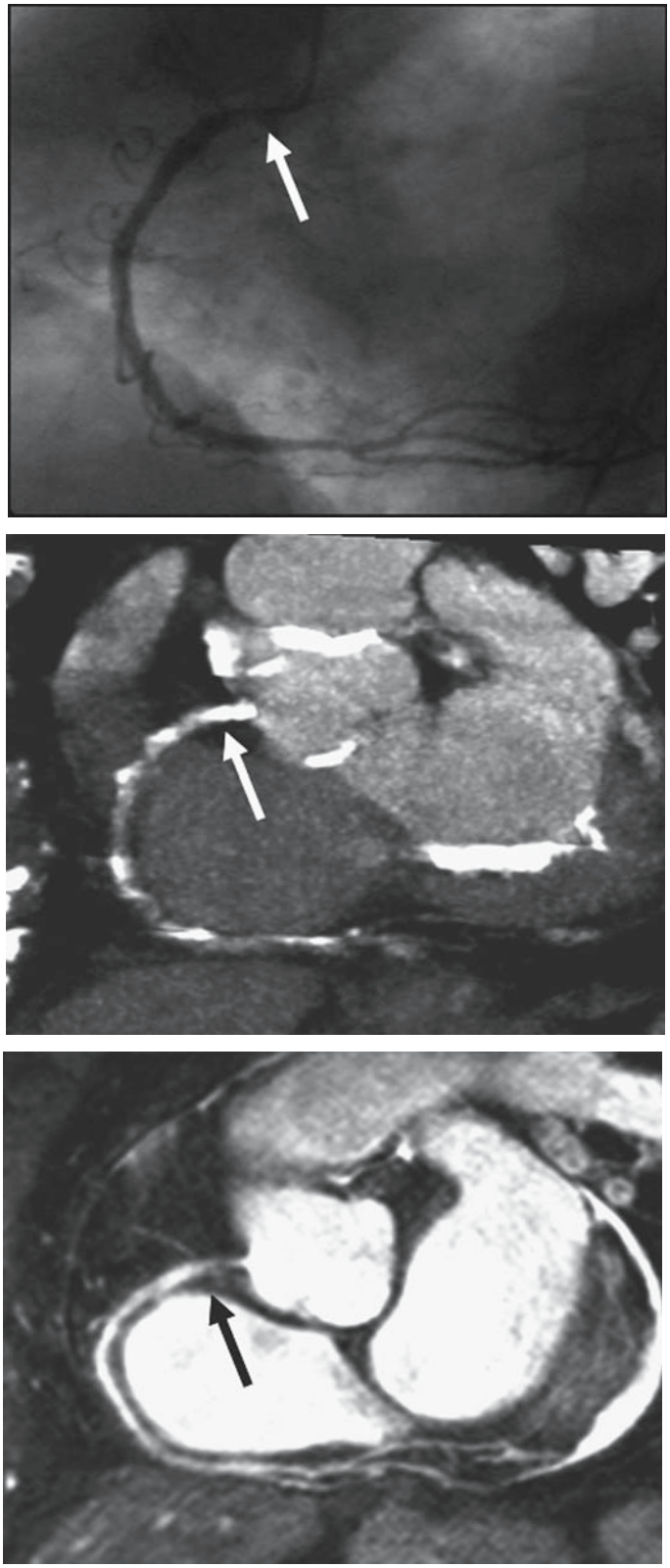

FIGURE 7.14. Right coronary artery (A) projection x-ray angiogram, (B) 16-slice multidetector computed tomography (MDCT), and (C) coronary MRI in a patient with prominent epicardial calcium. Note that the ostial right coronary artery (RCA) stenosis (arrow) is visible on the x-ray angiogram and the coronary MRI, but not on the MDCT.

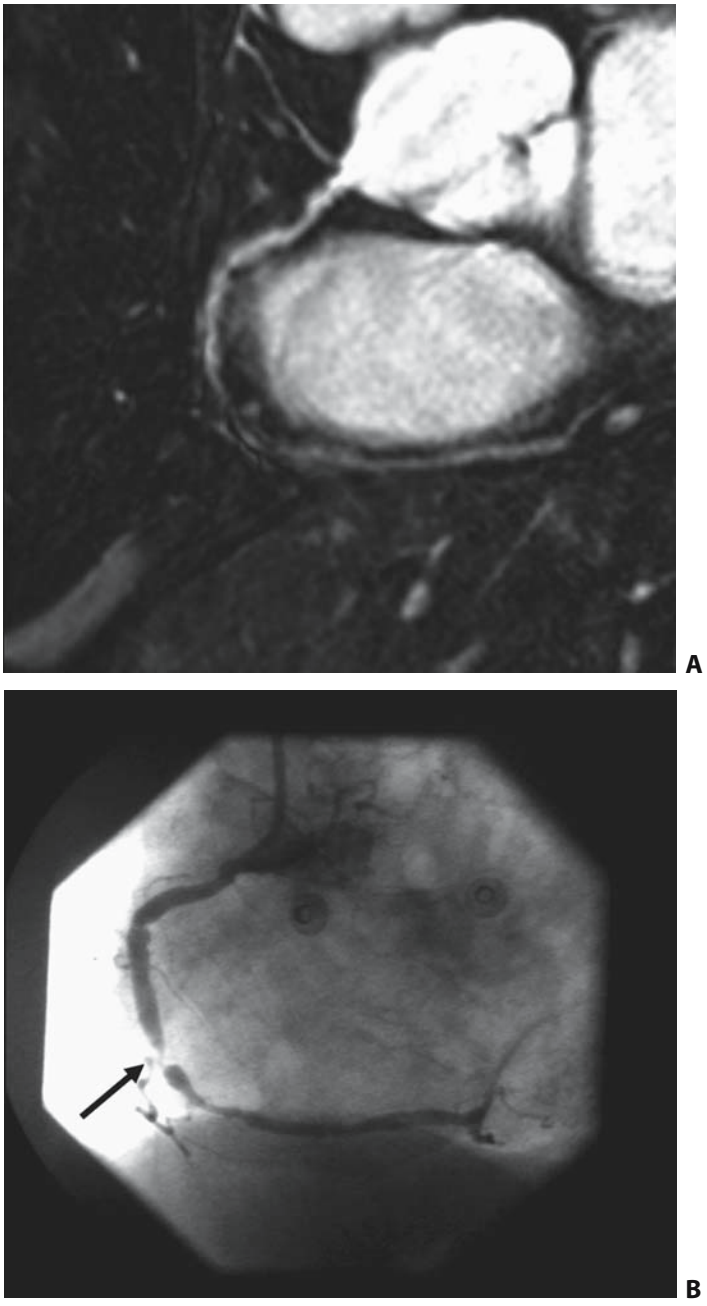

FIGURE 7.15. RCA (A) targeted 3D free breathing navigator coronary MRI and corresponding (B) projection x-ray angiogram in a patient with a mid-RCA stenosis (arrow).

ratio (CNR) with SSFP whole heart acquisitions,[85,86] but similar diagnostic results.[84,86] Preliminary data suggest similar overall results with 3T coronary MRI.[87] It is very likely that coronary MRI methods will get faster and more automated with subsequent application of powerful CT analytic tools to the 3D CMR data sets.

Although not yet routine due to issues of spatial resolution, another advantage of coronary MRI (vs. coronary CTA) is the application of phase velocity flow methods to assess coronary artery blood flow and flow reserve. For patients who

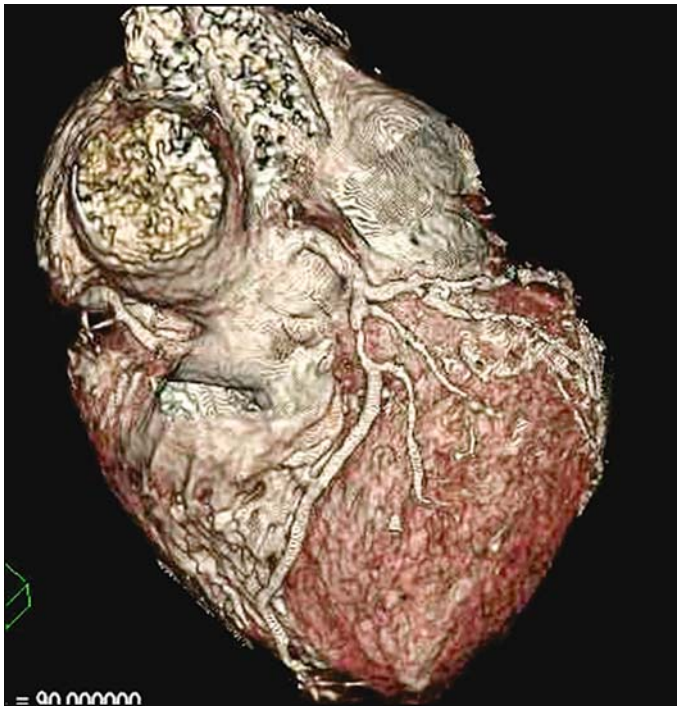

FIGURE 7.16. Whole heart coronary MRI reconstruction in a patient with a proximal left anterior descending branch (LAD) stenosis.

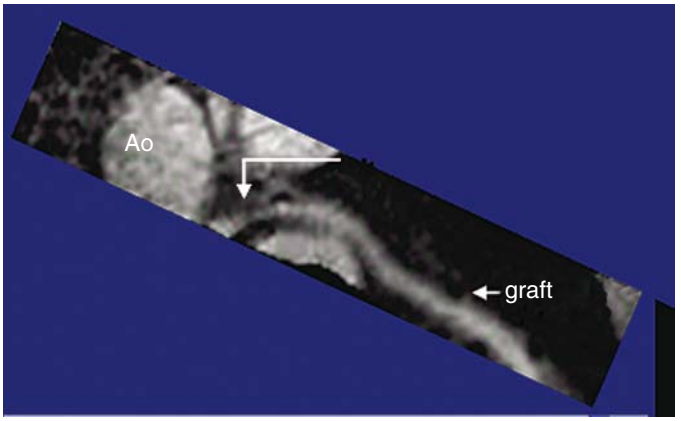

A

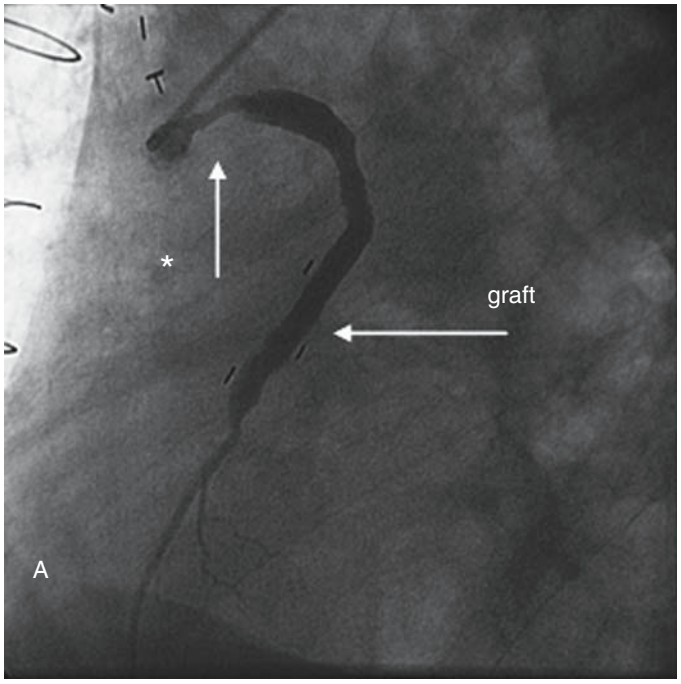

B

FIGURE 7.17. (A) Targeted 3D free breathing navigator coronary MRI and corresponding (B) projection x-ray angiogram in a patient with a stenosis (arrow) of a saphenous vein graft. Ao, aorta.

have experienced a myocardial infarction, phase velocity CMR can accurately evaluate the presence of antegrade flow in the infarct-related artery.[88] The noninvasive determination of patency influences therapy and prognosis in these patients.

Coronary Artery Bypass Graft Patency

In comparison with native vessel coronary MRI, CMR of coronary artery bypass grafts (both saphenous veins and internal mammary arteries) is facilitated by their relatively stationary anterior location, straight and predictable course, and their greater lumen diameter. Adequate flow is visualized as a signal void (spin-echo) or as bright signal (gradient-echo, contrast imaging) in the anatomic location corresponding to the expected graft position. Identification of flow in at least two contiguous slices, or obtained at different planes perpendicular to the expected bypass graft course suggests patency. If flow is suggested at only one level, graft patency is considered "indeterminate," and if there is no evidence of flow in any portions of the graft, the graft is considered "occluded." Spin-echo (dark blood), gradient-echo (bright blood), and Gd-DTPA–enhanced 3D coronary MRI have been reported to have higher sensitivity (95–100%) for patency of both saphenous venous and internal mammary grafts.[89–93] Focal disease can be identified using a 3D coronary MRI sequence[94] (Fig. 7.17). The addition of phase velocity imaging of graft flow[95] is also useful for discriminating vein graft patency, especially for jump grafts.

Implanted metallic clips, markers (Fig. 7.2), or intracoronary stents[15,96] (Fig. 7.3) will have a local signal void, precluding assessment in these regions. These artifacts, which are commonly located in very close proximity to the coronary arteries or grafts, preclude the assessment of these vessels. As mentioned earlier, both drug eluding stents currently marketed in the United States are FDA approved for CMR scanning immediately after implantation.

Myocardial Viability

Few applications of CMR have been so rapidly embraced by the clinical community as its ability to characterize myocardial fibrosis and thereby derive prognostic data regarding physiologic viability—the likelihood that resting regional left ventricular dysfunction will improve with mechanical revascularization. Extensive correlative CMR and histologic

studies in animal models have demonstrated that extracellular Gd-DTPA will localize/concentrate to areas corresponding to scar/fibrosis on histology and can be recognized using delayed enhancement CMR imaging.[97,98] Using an inversion recovery sequence with imaging 10 to 20 minutes following injection of 0.1 to 0.2 mmol/kg of Gd-DTPA, areas of hyperenhancement correspond to scar/fibrosis (Fig. 7.11) with highly reproducible results.[99] Delayed-enhancement CMR studies have demonstrated that the lack of hyperenhancement is a very strong predictor of functional viability (Fig. 7.13), while the presence of more than 50% transmural hyperenhancement is a powerful predictor for the lack of functional recovery.[100–102] An intermediate finding (1% to 49% transmurality) is less useful. For this group, regional systolic response to low-dose dobutamine appears superior[58] (Fig. 7.13). Delayed-enhancement CMR also compares favorably with electromechanical mapping[103] and clinical positron emission tomography.[104]

The DE-CMR method appears to be particularly superior to wall thinning for the discrimination of viable myocardium. Anecdotal reports[105] and preliminary data from a multicenter series[106] reported that 20% of subjects with thinned, akinetic segments have lack of hyperenhancement of those segments. Following mechanical revascularization, these segments demonstrate markedly improved systolic thickening in addition to local hypertrophy/normalization of diastolic wall thickness. Delayed-enhancement CMR also appears to be superior to global left ventricular ejection fraction for identification of patients with underlying substrate for sustained ventricular tachycardia.[107]

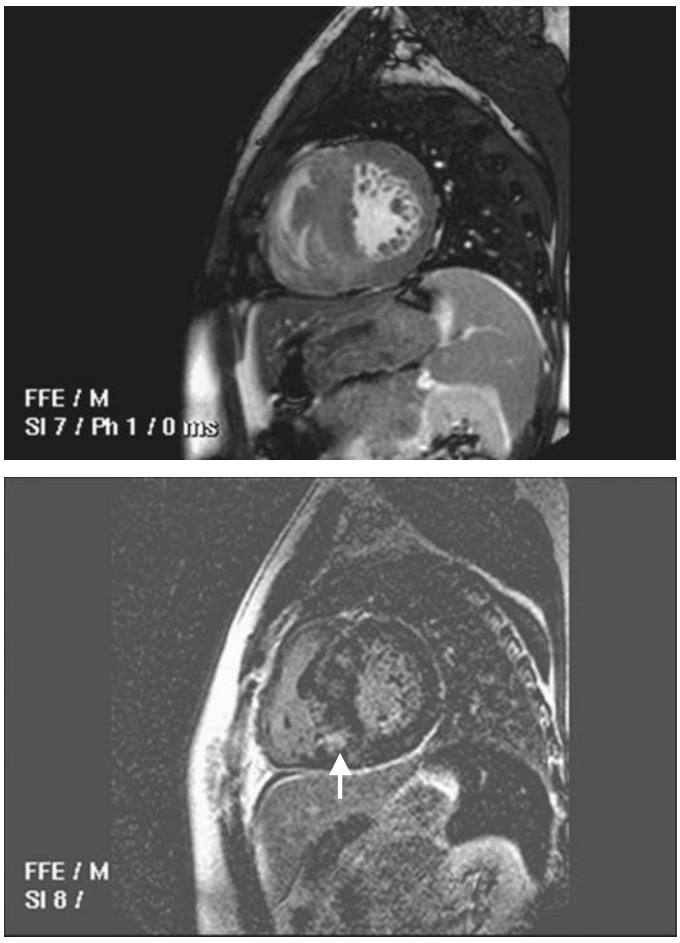

FIGURE 7.18. (A) Cine steady-state free precession (SSFP) short axis and corresponding (B) DE-CMR in a 17-year-old patient with hypertrophic cardiomyopathy. Note the prominent septal hypertrophy with an area of hyperenhancement at the juncture of the right ventricular free wall and septum (arrow).

Nonischemic Cardiomyopathies

Initial studies suggested that hyperenhancement may be specific for coronary artery disease.[108] Subsequent studies have shown that hyperenhancement may occur in a variety of nonischemic myopathic conditions including hypertrophic cardiomyopathy[109–111] (Fig. 7.18), Fabry's disease,[112] sarcoidosis,[113] myocarditis,[114,115] and Churg-Strauss syndrome.[116] A diffuse pattern of hyperenhancement is seen in amyloid cardiomyopathy.[117] Though not totally specific for myocardial infarction, a subendocardial hyperenhancement corresponding to a coronary artery distribution is far more common among patients with ischemic cardiomyopathy, while patients with nonischemic myopathies more often demonstrate a hyperenhancement pattern of the midventricular or epicardial layers that also do not correspond to a coronary distribution.[110,112,114–116] Two studies[83,118] have suggested that the pattern may be used to characterize the cause of a dilated cardiomyopathy, although 25% of patients with a "coronary disease" hyperenhancement pattern had a nonischemic myopathy. Thus, coronary MRI may be superior.[83] Among patients with a dilated cardiomyopathy given carvedilol, the absence of hyperenhancement predicts a regional improvement in systolic function, global improvement in left ventricular ejection fraction, and decrease in left ventricular cavity size.[119]

The ability of CMR to acquire images of the entire heart in true tomographic planes makes it ideal for the evaluation of patients with hypertrophic cardiomyopathies, especially important for evaluation of patients with focal/asymmetric hypertrophy (Fig. 7.18). Both DE-CMR[109–111] and investigative CMR "tagging" methods may assist in the assessment of these patients,[120] though the latter remains to be more fully elucidated. Serial CMR examinations may be useful to monitor ventricular remodeling and infarction size following alcohol ablation.[121]

In addition to biventricular volumetric and mass data, CMR may confirm excess iron deposition[122] as the cause of depressed systolic function in a patient with suspected hemochromatosis. Assessment of septal T2* has been shown to reflect myocardial iron stores, with T2* of less than 20 ms indicating iron overload.[123]

Cardiovascular magnetic resonance's ability to identify focal areas of fat and fibrosis is particularly valuable in the evaluation of patients with suspected arrhythmogenic right ventricular cardiomyopathy. This condition, in which the right ventricular free wall myocardium is diffusely or focally replaced with fatty or fibrous tissue with cavity dilation and focal wall thinning (or aneurysm), is associated with ventricular arrhythmias and sudden death. Spin-echo MRI can

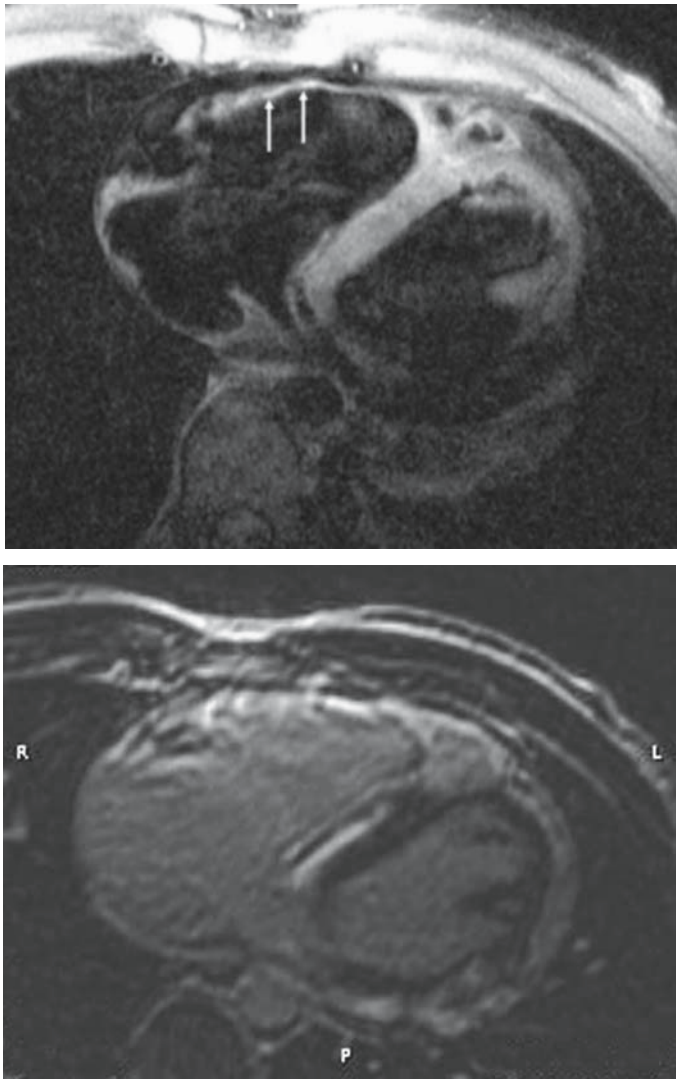

FIGURE 7.19. (A) Spin-echo CMR. Note the bright signal in the thinned right ventricular free wall (arrow) consistent with fatty infiltration. (B) Delayed enhancement imaging after administration of Gd-DTPA with enhancement of the right ventricular free wall.

be used to identify transmural or focal fatty infiltration in the right ventricular free wall as well as focal wall thinning (Fig. 7.19).[124,125] Delayed-enhancement CMR with right ventricular free wall hyperenhancement has also been described,[126] with the clinical history best able to discriminate hyperenhancement due to right ventricular infarction from that of a primary cardiomyopathy.

Valvular Heart Disease

The clinical adoption of CMR in the care of patients with valvular heart disease is expanding. Once almost solely the province of 2D and Doppler echocardiography, the unique quantitative nature of CMR with regard to ventricular volumes and function, as well as the ease in calculation of regurgitant volumes, has brought CMR to the clinical arena for the care of this large group of patients. Valve morphology (e.g., bicuspid valve) is easily recognized by CMR with acquisition of a cine SSFP data set through the plane of the aortic valve. For now, leaflet thickening, calcification, vegetations, abscess, and minor degrees of mitral valve prolapse largely remain the province of echocardiography, though obvious prolapse and partial leaflet flail are readily identified on cine CMR imaging.

For the assessment of aortic valve stenosis, two CMR approaches are utilized: a morphologic/2D assessment with planimetry of the maximum systolic aortic valve area[127] on orthogonal cine SSFP sequences, and a continuity equation "equivalent."[128] Difficulties with the anatomic (2D measures) include orientation of the slice among patients with markedly deformed valves, while difficulties with the continuity equation approach include orientation of the imaging plane perpendicular to the maximal velocity jet and dephasing/artifacts due to turbulence in patients with severe aortic stenosis. Analogous approaches are used for assessing mitral stenosis, including 2D planimetry of the mitral valve area as defined by a cine acquisition oriented orthogonal to the valve plane[129] and with the use of phase velocity mapping at the level of the mitral leaflet tips,[130] thereby applying a pressure-half-time equivalent measurement. Difficulties with the former again include proper orientation orthogonal to flow, while limitations of the latter include the relatively poor temporal (vs. Doppler echocardiography) resolution and diastolic artifacts among the many patients with coexistent mitral stenosis and atrial fibrillation.

The use of CMR for the quantitative assessment of valvular regurgitation is much more direct and highly quantitative. Qualitative assessment of mitral and aortic regurgitation had initially been by qualitative estimate of the flow disturbance (signal void) in the receiving chamber in a manner somewhat analogous to color Doppler. These early studies showed a good correlation with Doppler echocardiography.[131] However, the subsequent introduction of strong gradients and shorter echo times led to attenuation and near elimination of the dephasing artifact.[132] This is particularly true of the newer SSFP acquisitions, which have become "standard" at most CMR centers, with the nearly complete elimination of regurgitant jets. Fortunately, CMR offers a more quantitative approach. Using phase velocity mapping, flow is measured across the aortic valve (from a practical perspective, this is often obtained in the axial plane at the level of the bifurcation of the pulmonary artery). Such an assessment includes a direct quantitative assessment of aortic regurgitation (Fig. 7.20). For mitral regurgitation, we generally quantify the mitral regurgitant volume as the difference between the left ventricular stroke volume (derived from the contiguous short axis left ventricular stack) and the forward flow out of the aorta. Another option is to directly measure mitral regurgitation volume using phase velocity mapping at the level of the mitral annulus. We have found the latter approach to be technically more challenging due to the base to apex motion of the annulus during systole and eccentric, high-velocity mitral regurgitation jets, which sometimes lead to errors, analogous to some of the limitations of quantitative Doppler echocardiography.

Beyond simple calculation of regurgitant volume, CMR provides for the ready determination of regurgitant fraction (regurgitant volume/stroke volume), regurgitant volume index (regurgitant volume/end-diastolic volume), and effec-

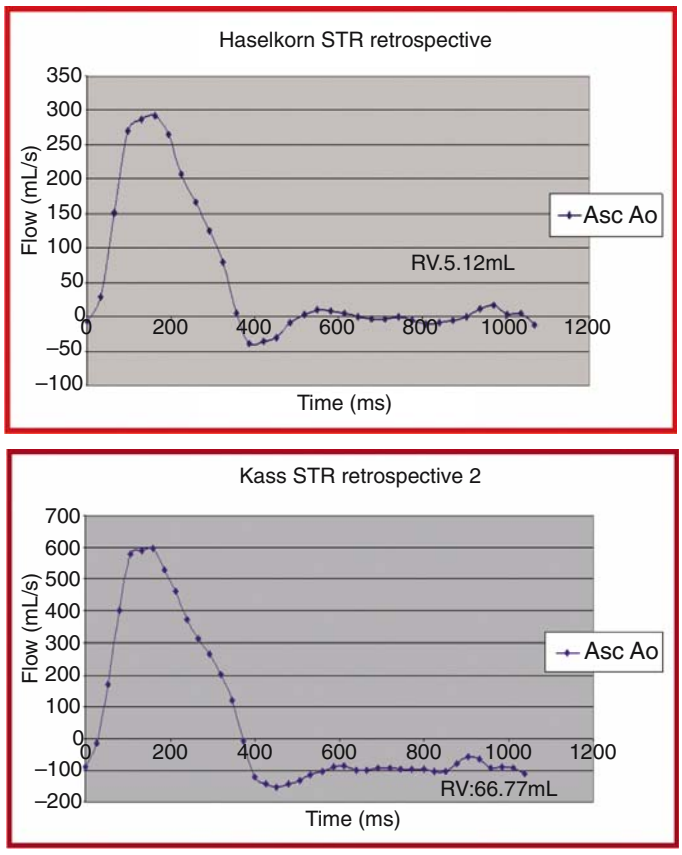

FIGURE 7.20. Integrated phase velocity data acquired in the proximal ascending aorta (Asc Ao) in a patient (A) without and (B) with severe aortic regurgitation. Note the persistence of "negative" flow throughout diastole in the patient with severe aortic regurgitation with a total of 56 mL of aortic regurgitation.

tive forward ejection fraction (net forward stroke volume/end-diastolic volume). These same measures can be equally well applied for pulmonic and tricuspid regurgitation. Another advantage of CMR versus echocardiography and invasive measures is the ability to easily quantify the regurgitant volumes attributable to each valve in the presence of serial regurgitant lesions (e.g., mitral regurgitation and aortic regurgitation).

Cardiac Tumors and Masses

Although the high spatial resolution of CMR allows for depiction of intracavitary tumors/masses (e.g., myxoma), these intracavitary "masses" are generally well appreciated and characterized using conventional echocardiography (transthoracic or transesophageal). However, the sensitivity and accuracy of transthoracic echocardiography for mural left ventricular thrombi has recently been called into question by an operative series that suggested far superior accuracy of DE-CMR (Fig. 7.11).[49,50] Cardiovascular magnetic resonance also has great value for characterizing paracardiac and extracardiac tumors[133] and their extension into the myocardium, cardiac chambers, or neighboring mediastinal structures (e.g., vena cavae, pulmonary veins). The ability of 3D CMR data sets to be reconstructed in any orientation helps to guide the surgical approach in such situations.

Though rarely difficult to diagnose from echocardiographic images, benign lipomatous hypertrophy of the interatrial septum as visualized on transthoracic echocardiography (TTE) or TEE may sometimes lead to the misdiagnosis of an atrial septal "tumor." The characteristic, very intense signal from fatty tissue[134] with suppression using a fat saturation prepulse readily allows for the CMR diagnosis of this benign disorder.

Pericardium

The normal pericardium extends around the heart as a thin black line between visceral and parietal pericardial fat on spin-echo CMR imaging. Normal pericardial thickness is 3 mm or less.[135] Among patients presenting with constrictive cardiomyopathy, often following recurrent pericarditis or mediastinal radiation, the pericardium is thickened (Fig. 7.21), a finding that is readily appreciated by ECG-triggered spin-echo CMR. Gradient-echo methods are slightly less reliable for pericardial thickness.[136] Computed tomography is also valuable in this situation, and is better suited for the specific assessment of pericardial *calcifications* (see Chapter 67). It should be remembered, however, that while CMR (and CT) will accurately quantify focal pericardial thickening, the presence of thickened pericardium alone is not diagnostic of constrictive physiology, and constriction may be present in the absence of pericardial thickening.[137] Cardiovascular magnetic resonance tagging methods demonstrate adherence of the pericardium to underlying epimyocardium.[138] Among patients with constriction, CMR also frequently demonstrates thickened pericardium in concert with an enlarged inferior vena cava alone, right atrial and right ventricular enlargement,[136] and abnormal septal motion (with real-time CMR). Though echocardiography is generally adequate for circumferential effusions, CMR depicts transudative effusions as areas of high intensity and may be particularly

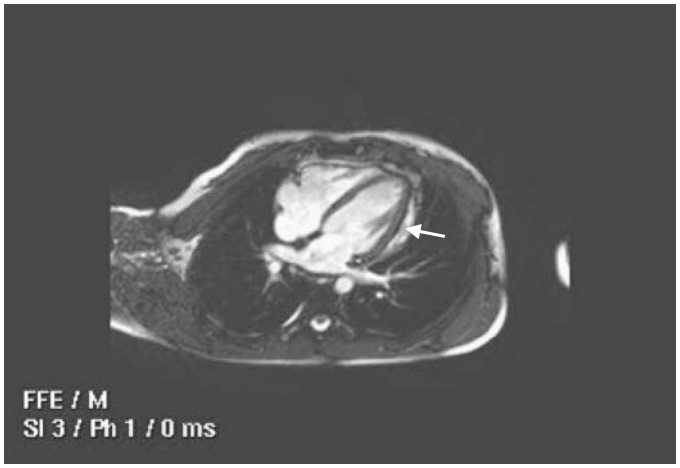

FIGURE 7.21. Cine four-chamber SSFP image in a 45-year-old man with recurrent pericarditis and symptoms of constriction. Note the thickened pericardium with fluid (arrow) and stranding within the pericardial space.

helpful in the delineation of loculated effusions, especially in patients with suboptimal echocardiographic windows. Delineation of hemorrhagic and transudative effusions is another attribute of CMR.

Congenital Heart Disease

An extensive review of CMR applications for congenital heart disease is beyond the scope of this chapter. As previously mentioned, CMR has great utility for both simple and complex congenital heart disease. While hemodynamically significant atrial septal defects and ventricular septal defects are usually identifiable by TTE or TEE, phase-velocity CMR is highly accurate and valuable for *quantifying* the pulmonary/systemic flow ratio in patients with known defects[139] and characterizing congenital heart disease outside of the cardiac chambers. These defects include aortic coarctation (Fig. 7.6), anomalous pulmonary venous drainage (Table 7.1; Fig. 7.22), and complex congenital heart disease in patients who have undergone corrective or palliative surgery. For these patients, CMR defines structural components and their relationships, including serial evaluation and planning of subsequent surgical interventions.

Coronary MRI for identification and characterization of anomalous coronary arteries is widely accepted as a clinical tool. This condition is found in less than 2% of the population and is generally benign. However, there is an increased risk of sudden death and myocardial infarction when the anomalous vessel courses between the aorta and pulmonary artery (Fig. 7.23). Even among patients with anomalous coronary arteries identified by invasive x-ray angiography, the anatomic course of the vessel may be misinterpreted owing to the projection method or operator inexperience, especially with the declining routine use of right heart catheterization, making coronary MRI a preferred approach. Several studies have now reported on the value of MR in this condition,[140–143] including the finding of initial misinterpretation by conventional x-ray angiography.[141,143] Though coronary MRI data for anomalous disease are quite extensive, in the absence of a strong suspicion, data are not sufficient to support routine coronary CMR screening among young adults who present with chest pain. Coronary CTA likely has similar efficacy, though it has been less well studied and would expose young adults to potentially harmful ionizing radiation.

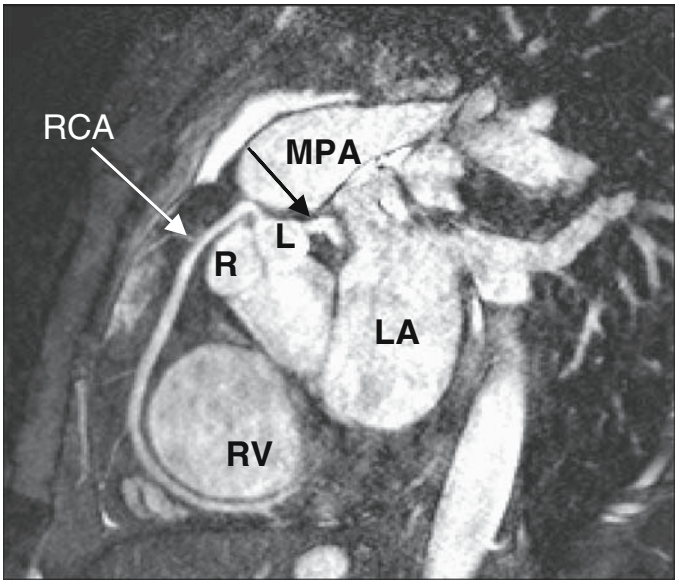

FIGURE 7.23. Reconstruction of targeted 3D free-breathing navigator coronary MRI in a patient with an anomalous right coronary artery of the "malignant" form originating from the left (L) coronary cusp. LA, left atrium; MPA, main pulmonary artery; R, right coronary cusp; RV, right ventricle.

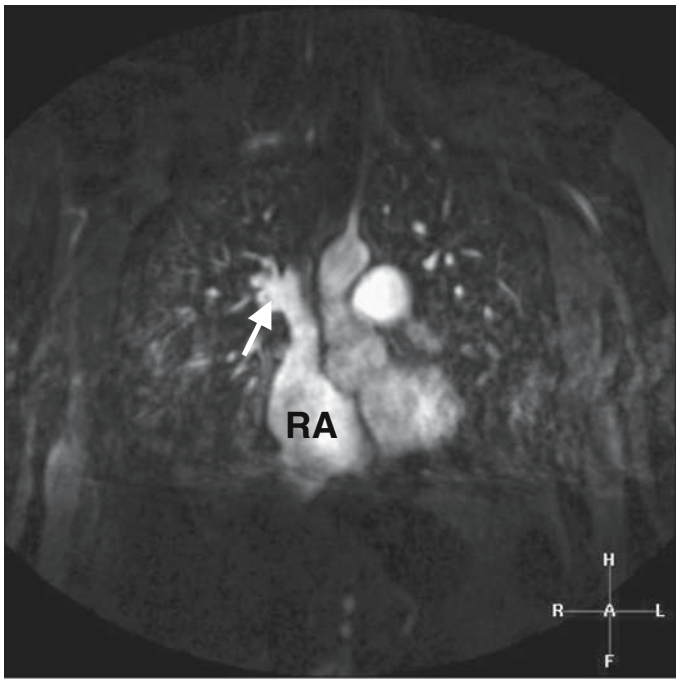

FIGURE 7.22. A 3D CE-MRA in a patient with an anomalous pulmonary vein (solid arrow) entering the superior vena cava (dashed arrow). RA, right atrium.

Summary

Over the past decade, there has been tremendous clinical growth in CMR. The recent introduction of high field (e.g., 3 T) CMR systems[144] and application of parallel imaging methods[145] in CMR has the potential to dramatically decrease the time needed for CMR study completion. Moreover, investigations in the use of CMR for detection of subclinical disease are ongoing[146] and expected to further expand the role of CMR in clinical care. Finally, the enhancement of real-time CMR has facilitated the exciting birth of interventional CMR methods, including placement of percutaneous valves and atrial septal defect closure devices as well as guidance for electrophysiologic procedures. Intervention CMR is expected to have its greatest initial impact in the pediatric population,[147] for which radiation exposure is of greatest concern.

References

1. Pennell DJ, Sechtem UP, Higgins CB, et al. Clinical indications for cardiovascular magnetic resonance (CMR): Consensus Panel Report. J Cardiovasc Magn Reson 2004;6:727–765.
2. Plein S, Ridgway JP, Jones TR, Bloomer TN, Sivananthan MU. Coronary artery disease: assessment with a comprehensive MR imaging protocol—initial results. Radiology 2002;225: 300–307.
3. Foo TK, Ho VB, Saranathan M, et al. Feasibility of integrating high-spatial resolution 3D breath-hold coronary MR angiography with myocardial perfusion and viability examinations. Radiology 2005;235:1025–1030.
4. Pohost GM, Kim RJ, Kramer CM, Manning WJ. Task Force 12: Training in advanced cardiovascular imaging for Cardiovascular Magnetic Resonance. *J Am Coll Cardiol* 2006;47:910–914.
5. Pohost GM, Higgins CB, Grist T, et al. Guidelines for credentialing in cardiovascular magnetic resonance (CMR). J Card Magn Resonan 2000;2:233–234.
6. Weinreb JC, Larson PA, Woodard PK, et al. American College of Radiology Clinical Statement on Noninvasive Cardiac Imaging. Radiology 2005;235:723–727.
7. Budoff MJ, Cohen MC, Garcia MJ, et al. ACCF/AHA clinical competence statement on cardiac imaging with computed tomography and magnetic resonance. J Am Coll Cardiol 2005;46:383–402.
8. Balaban RS. The physics of image generation by magnetic resonance. In: Manning WJ, Pennell DJ, eds. Cardiovascular Magnetic Resonance. Philadelphia: Churchill Livingstone, 2002:3–17.
9. Edelman RR, Hesselink JR, Zlatkin MB, eds. Clinical Magnetic Resonance Imaging. Philadelphia: Elsevier-Saunders, 2006.
10. Edelman RR. Contrast-enhanced MR imaging of the heart: overview of the literature. Radiology 2004;232:653–668.
11. Goyen M, Debatin JF. Gadopentetate dimeglumine-enhanced three-dimensional MR-angiography: dosing, safety, and efficacy. J Magn Reson Imaging 2004;19:261–273.

11a. Sam AD, Morasch MD, Collins J, et al. Safety of gadolinium contrast angiography in patients with chronic renal insufficiency. J Vasc Surgery 2003;38:313–318.

12. Hundley WG, Meshack BM, Willett DL, et al. Comparison of quantitation of left ventricular volume, ejection fraction, and cardiac output in patients with atrial fibrillation by cine magnetic resonance imaging versus invasive measurements. Am J Cardiol 1996;78:1119–1123.
13. Kerr AB, Pauly JM, Hu BS, et al. Real-time interactive MRI on a conventional scanner. Magn Reson Med 1997;38:355–367.
14. Shellock FG. Reference Manual for Magnetic Resonance Safety, Implants, and Devices—2005. Philadelphia: WB Saunders, 2005.
15. Kramer CM, Rogers WJ, Pakstis DL. Absence of adverse outcomes after magnetic resonance imaging early after stent placement for acute myocardial infarction: a preliminary study. J Cardiovasc Magn Reson 2000;2:257–261.
16. Gimbel JR, Johnson D, Levine PA, Wilkoff BL. Safe performance of magnetic resonance imaging on five patients with permanent cardiac pacemakers. PACE 1996;19:913–919.
17. Martin ET, Coman JA, Shellock FG, et al. Magnetic resonance imaging and cardiac pacemaker safety at 1.5-Tesla. J Am Coll Cardiol 2004:43:1315–1324.
18. Roguin A, Zviman MM, Meininger GR, et al. Modern pacemaker and implantable cardioverter/defibrillator systems can be magnetic resonance imaging safe: in-vitro and in-vivo assessment of safety and function at 1.5T. Circulation 2004;110:475–482.
19. Nienaber CA, von Kodolitsch Y, Nicolas V, et al. The diagnosis of thoracic aortic dissection by noninvasive imaging procedures. N Engl J Med 1993;328:1:1–9.
20. Laissy JP, Blanc F, Soyer P, et al. Thoracic aortic dissection: diagnosis with transesophageal echocardiography versus MR imaging. Radiology 1995;194:331–316.
21. Goldfarb JW, Holland AE, Edelman RR. Single breath-hold multi-slap and CINE cardiac-synchronized gadolinium-enhanced three-dimensional angiography. Magn Reson Imaging 2001;17:434–451.
22. Prince MR, Narasimham DL, Jacoby WT, et al. Three-dimensional gadolinium-enhanced MR angiography of the thoracic aorta. AJR 1996;166:1387–1397.
23. Krinsky GA, Reuss PM, Lee VS, Carbognin G, Rofsky NM. Thoracic aorta: comparison of single-dose breath-hold and double-dose non-breath-hold gadolinium-enhanced three dimensional MR angiography. AJR 1999;173:145–150.
24. Murray JG, Manisali M, Flamm SD, et al. Intramural hematoma of the thoracic aorta: MR image findings and their prognostic implications. Radiology 1997;204:349–355.
25. Keren A, Kim CB, Hu BS, et al. Accuracy of biplane and multiplane transesophageal echocardiography in diagnosis of typical acute aortic dissection and intramural hematoma. J Am Coll Cardiol 1996;28:627–636.
26. Sommer T, Fehski W, Holzknecht N, et al. Aortic dissection: a comparative study of diagnosis with spiral CT, multiplanar transesophageal echocardiography, and MR imaging. Radiology 1996;199:347–352.
27. Cesare ED, Giordana AV, Cerone G, et al. Comparative evaluation of TEE, conventional MRI and contrast-enhanced 3D breath-hold MRA in the post-operative follow-up of dissecting aneurysms. Int J Card Imaging 2000;16:135–147.
28. Oshinski JN, Parks WJ, Markou CP, et al. Improved measurement of pressure gradients in aortic coarctation by magnetic resonance imaging. J Am Coll Cardiol 1996;28:1818–1826.
29. Hatabu H, Gaa J, Kim D, et al. Pulmonary perfusion and angiography: evaluation with breath-hold enhanced three-dimensional fast imaging steady-state precession MR imaging with short TR and TE. AJR 1996;167:653–655.
30. Meaney JF, Weg JG, Chenevert TL, et al. Diagnosis of pulmonary embolism with magnetic resonance angiography. N Engl J Med 1997;336:1422–1427.
31. Stern EJ, Graham C, Gamsu G, et al. Pulmonary artery dissection: MR findings. J Comput Assist Tomogr 1992;16:481–483.
32. Dill T, Neumann T, Ekinci O, et al. Pulmonary vein diameter reduction after radiofrequency catheter ablation for paroxysmal atrial fibrillation evaluated by contrast-enhanced three-dimensional magnetic resonance imaging. Circulation 2003; 107:845–850.
33. Hauser TH, Yeon SB, McClennen S, et al. A method for the determination of proximal pulmonary vein size using contrast enhanced magnetic resonance angiography. J Cardiovasc Magn Reson 2004;6:927–936.
34. Kato R, Lickfett L, Meininger G, et al. Pulmonary vein anatomy in patients undergoing catheter ablation of atrial fibrillation: lessons learned by use of magnetic resonance imaging. Circulation 2003;107:2004–2010.
35. Hauser TH, Yeon SB, McClennen S, et al. Subclinical pulmonary vein narrowing following ablation for atrial fibrillation. Heart 2005;91:672–673.

35a. Peters DC, Wylie J, Hauser TH, et al. Detection of pulmonary vein and left atrial scar after catheter ablation using 3D navigator-gated delayed enhancement magnetic resonance imaging – initial experience. Radiology 2006 (in press).

36. Chuang ML, Hibberd MG, Salton CJ, et al. Importance of imaging method over imaging modality in noninvasive determination of left ventricular volumes and ejection fraction:

assessment by two and three-dimensional echocardiography and magnetic resonance imaging. J Am Coll Cardiol 2000;35: 477–484.
37. Caiani EG, Corsi C, Zamorano J, et al. Improved semiautomated quantification of left ventricular volumes and ejection fraction using 3–dimensional echocardiography with a full matrix-array transducer: comparison with magnetic resonance imaging. J Am Soc Echocardiogr 2005;18:779–788.
38. Burgstahler C, Heuschmid M, Rothfuss J-K, et al. Noninvasive evaluation of global left ventricular myocardial function with ECG-gated 16–slice multidetector computed tomography in comparison with magnetic resonance. Circulation 2004;110: III-573–574(abstr).
39. Cranney GB, Lotan CS, Dean L, Baxley W, et al. Left ventricular volume measurement using cardiac axis nuclear magnetic resonance imaging: validation by calibrated ventricular angiography. Circulation 1990 82:154–163.
40. Mogelvang J, Stokholm KH, Saunamaki K, Reimer A, et al. Assessment of left ventricular volumes by magnetic resonance in comparison with radionuclide angiography, contrast angiography and echocardiography. Eur Heart J 1992;13:1677–1683.
41. Sakuma H, Fujita N, Foo TKF, et al. Evaluation of left ventricular volume and mass with breath-hold cine MR imaging. Radiology 1993;188:377–380.
42. Grothues F, Smith GC, Moon JC, et al. Comparison of interstudy reproducibility of cardiovascular magnetic resonance with two-dimensional echocardiography in normal subjects and in patients with heart failure or left ventricular hypertrophy. Am J Cardiol 2002;90:29–34.
43. Petersen SE, Selvanayagam JB, Wiesmann F, et al. Left ventricular non-compaction: insights from cardiovascular magnetic resonance. J Am Coll Cardiol 2005;46:101–105.
44. Harrity P, Patel A, Bianco J, Subramanian R. Improved diagnosis and characterization of postinfarction left ventricular pseudoaneurysm by cardiac magnetic resonance imaging. Clin Cardiol 1991;14:603–606.
45. Bellenger NG, Burgess M, Ray SG, et al. Comparison of left ventricular ejection fraction and volumes in heart failure by two-dimensional echocardiography, radionuclide ventriculography and cardiovascular magnetic resonance. Eur Heart J 2000;21:1387–1396.
46. Johnson DB, Foster RE, Barilla F, et al. Angiotensin-converting enzyme inhibitor therapy affects left ventricular mass in patients with ejection fraction >40% after acute myocardial infarction. J Am Coll Cardiol 1997;29:49–54.
47. Cerqueira MD, Weissman NJ, Dilsizian V, et al. Standardized myocardial segmentation and nomenclature for tomographic imaging of the heart: a statement for healthcare professionals from the Cardiac Imaging Committee of the Council on Clinical Cardiology of the American Heart Association. Circulation 2002;105:539–542.
48. McNamara MT, Higgins CB. Magnetic resonance imaging of chronic myocardial infarctions in man. AJR 1986;146:315–320.
49. Mollet NR, Dymarkowski S, Volders W, et al. Visualization of ventricular thrombi with contrast-enhanced magnetic resonance imaging in patients with ischemic heart disease. Circulation 2002;106:2873–2876.
50. Srichai MB, Junor C, Rodriguez L, et al. Imaging and pathologic characteristics of left ventricular thrombus: a comparison of contrast-enhanced magnetic resonance imaging, transthoracic echocardiography, and transesophageal echocardiography with surgical or pathologic validation. Circulation 2004;110: III-404(abstr).
51. Grothues F, Moon JC, Bellenger NG, et al. Interstudy reproducibility of right ventricular volumes, function, and mass with cardiovascular magnetic resonance. Am Heart J 2004; 147:218–223.
52. Fayad ZA, Ferrari VA, Kraitchman DL, et al. Right ventricular regional function using MR tagging: normals versus chronic pulmonary hypertension. Magn Reson Med 1998;39: 116–123.
53. Kramer CM, Rogers WJ, Theobald TM, et al. Remote noninfarcted region dysfunction soon after first anterior myocardial infarction. A magnetic resonance tagging study. Circulation 1996;94:660–666.
54. Roest AA, Kunz P, Lamb HJ, et al. Biventricular response to supine physical exercise in young adults assessed with ultrafast magnetic resonance imaging. Am J Cardiol 2001;87:601–605.
55. Nagel E, Lehmkuhl HB, Bocksch W, et al. noninvasive diagnosis of ischemia-induced wall motion abnormalities with the use of high dose dobutamine stress MRI: comparison with dobutamine echocardiography. Circulation 1999;99:763–770.
56. Hundley WG, Hamilton CA, Thomas MS, et al. utility of fast cine magnetic resonance imaging and display for the detection of myocardial ischemia in patients not well suited for second harmonic stress echocardiography. Circulation 1999; 100:1697–1702.
57. Schalla S, Klein C, Paetsch I, et al. Real-time MR image acquisition during high-dose dobutamine hydrochloride stress for detecting left ventricular wall motion abnormalities in patients with coronary arterial disease. Radiology 2002;224:845–851.
58. Paetsch I, Jahnke C, Wahl A, et al. Comparison of dobutamine stress magnetic resonance, adenosine stress magnetic resonance, and adenosine stress magnetic resonance perfusion. Circulation 2004;110:835–842.
59. Hundley WG, Morgan TM, Neagle CM, et al. Magnetic resonance imaging determination of cardiac prognosis. Circulation 2002:106:2328–2333.
60. Kuijpers D, Ho KY, van Dijkman PR, et al. Dobutamine cardiovascular magnetic resonance for the detection of myocardial ischemia with the use of myocardial tagging. Circulation 2003;107:1592–1597.
61. Al-Saadi N, Nagel E, Gross M, et al. Non-invasive detection of myocardial ischemia from perfusion reserve based on cardiovascular magnetic resonance. Circulation 2000;101:1379–1383.
62. Wilke N, Simm C, Zhang J, et al. Contrast enhanced first pass myocardial perfusion imaging: correlation between myocardial blood flow in dogs at rest and during hyperemia. Magn Reson Med 1993;29:485–497.
63. Epstein FH, London JF, Peters DC, et al. Multislice first-pass cardiac perfusion MRI: validation in a model of myocardial infarction. Magn Reson Med 2002;47:482–491.
64. Wolff SD, Schwitter J, Coulden R, et al. Myocardial first-pass perfusion magnetic resonance imaging. A multicenter dose-ranging study. Circulation 2004;110:732–737.
65. Panting JR, Gatehouse PD, Yang GZ, et al. Echo planar magnetic resonance myocardial perfusion imaging: parametric map analysis and comparison with thallium SPECT. J Magn Reson Imaging 2001;13:192–200.
66. Schwitter J, Nanz D, Kneifel S, et al. Assessment of myocardial perfusion in coronary artery disease by magnetic resonance: a comparison with positron emission tomography and coronary angiography. Circulation 2001;103:2230–2235.
67. Al-Saadi N, Nagel E, Gross M, et al. Improvement of myocardial perfusion reserve early after coronary intervention: assessment with cardiac magnetic resonance imaging. J Am Coll Cardiol 2000;36:1557–1564.
68. Panting JR, Gatehouse PD, Yang GZ, et al. Abnormal subendocardial perfusion in cardiac syndrome-X detected by cardiovascular magnetic resonance imaging. N Engl J Med 2002; 346:1948–1953.
69. Hunold P, Vogt FM, Schmermund A, et al. Radiation exposure during cardiac CT: effective doses at multidetector row CT and electron-beam CT. Radiology 2003;226:145–152.

70. Shaw LJ, Raggi P, Schisterman E, Berman DS, Callister TQ. Prognostic value of cardiac risk factors and coronary artery calcium screening for all-cause mortality. Radiology 2003;228:826–833.
71. Hoffman U, Moselewski F, Cury RC, et al. Predictive value of 16–slice multidetector spiral computed tomography to detect significant obstructive coronary disease in patients at high risk for coronary artery disease. Circulation 2004;110:2638–2643.
72. Maintz D, Ozgun M, Hoffmeier A, Botnar R, Fischbach R, Heindel W. Comparison of whole heart coronary MR angiography and coronary CT angiography [abstr]. Radiology 2004; (suppl):273.
73. Manning WJ, Li W, Edelman RR. A preliminary report comparing magnetic resonance coronary angiography with conventional angiography. N Engl J Med 1993;328:828–832.
74. Duerinckx AJ, Urman MK. Two-dimensional coronary MR angiography: analysis of initial clinical results. Radiology 1994;193:731–738.
75. Pennell DJ, Bogren HG, Keegan J, Firmin DN, Underwood SR. Assessment of coronary artery stenosis by magnetic resonance imaging. Heart 1996;75:127–133.
76. Sommer T, Hackenbroch M, Hofer U, Meyer C, Flacke S, Schild H. Submillimeter 3D coronary MR angiography with real-time navigator correction in 112 patients with suspected coronary artery disease. J Cardiovasc Magn Reson 2001;4:28(abstr).
77. Bogaert J, Kuzo R, Dymarkowski S, et al. Coronary artery imaging with real-time navigator three-dimensional turbo-field-echo MR coronary angiography: initial experience. Radiology 2003;226:707–716.
78. Botnar RM, Stiuber M, Danias PG, et al. Improved coronary artery definition with T2–weighted, free breathing, three dimensional coronary MRA. Circulation 1999;99:3139–3148.
79. Jahnke C, Paetsch I, Schnackenburg B, et al. Coronary MR angiography with steady-state free precession: individually adapted breath-hold technique versus free-breathing technique. Radiology 2004:232:669–676.
80. Plein S, Jones TR, Ridgway JP, Sivananthan MU. Three-dimensional coronary MR angiography performed with subject-specific cardiac acquisition windows and motion-adapted respiratory gating. AJR 2003;180:505–512.
81. Kefer J, Coch E, Legros G, et al. Head-to-head comparison of three-dimensional navigator-gated magnetic resonance imaging and 16-slice computed tomography to detect coronary artery stenosis in patients. J Am Coll Cardiol 2005;46:92–100.
82. Kim WY, Danias PG, Stuber M, et al. Coronary magnetic resonance angiography for the detection of coronary stenosis. N Engl J Med 2001;345:1863–1869.
83. Hauser TH, Yeon SB, Appelbaum E, et al. Discrimination of ischemic vs. non-ischmemic cardiomyopathy among patients with heart failure using combined coronary MRI and delayed enhancement CMR. J Cardiovasc Magn Resonan 2005;7: 94(abstr).
84. Maintz D, Aepfelbacher FC, Kissinger KV, et al. Coronary magnetic resonance angiography: Comparison of quantitative and qualitative data among four techniques. AJR 2004;182: 515–521.
85. Weber OM, Martin AJ, Higgins CB. Whole-heart steady-state free precession coronary artery magnetic resonance angiography. Magn Reson Med 2003;50:1223–1228.
86. Ichikawa Y, Sakuma H, Makino K, et al. Diagnostic accuracy of whole heart coronary magnetic resonance angiography for the detection of significant coronary stenosis in patients with suspected coronary artery disease. J Cardiovasc Magn Reson 2005;7:60(abstr).
87. Sommer T, Hackenbroch M, Hofer U, et al. Coronary MR angiography at 3.0 T versus that at 1.5 T: initial results in patients suspected of having coronary artery disease. Radiology 2005: 234:718–725.
88. Hundley WG, Clarke GD, Landau C, et al. Noninvasive determination of infarct artery patency by cine magnetic resonance angiography. Circulation 1995;91:1347–1353.
89. White RD, Caputo GR, Mark AS, Modin GW, Higgins CB. Coronary artery bypass graft patency: noninvasive evaluation with MR imaging. Radiology 1987;164:681–686.
90. Rubinstein RI, Askenase AD, Thickman D, Feldman MS, Agarwal JB, Helfhant RH. Magnetic resonance imaging to evaluate patency of aortocoronary bypass grafts. Circulation 1987;76:786–791.
91. Aurigemma GP, Reichek N, Axel L, Schiebler M, Harris C, Kressel HY. Noninvasive determination of coronary artery bypass graft patency by cine magnetic resonance imaging. Circulation. 1989;80:1595–1602.
92. Galjee MA, van Rossum AC, Doesburg T, van Eenige MJ, Visser CA. Value of magnetic resonance imaging in assessing patency and function of coronary artery bypass grafts. An angiographically controlled study. Circulation 1996;93:660–666.
93. Vrachliotis TG, Bis KG, Aliabadi D, Shetty AN, Safian R, Simonetti O. Contrast-enhanced breath-hold MR angiography for evaluating patency of coronary artery bypass grafts. AJR 1997;168:1073–1080.
94. Langerak SE, Vliegen HW, de Roos A, et al. Detection of vein graft disease using high-resolution magnetic resonance angiography. Circulation 2002;105:328–333.
95. Langerak SE, Kunz P, Vliegen HW, et al. MR flow mapping in coronary artery bypass grafts: a validation study with Doppler flow measurements. Radiology 2002;222:127–135.
96. Duerinckx AJ, Atkinson D, Hurwitz R, et al. Coronary MR angiography after coronary stent placement. AJR 1995;165: 662–664.
97. Fieno DS, Kim RJ, Chen EL, et al. Contrast-enhanced magnetic resonance imaging of myocardium at risk: distinction between reversible and irreversible injury throughout infarct healing. J Am Coll Cardiol 2000;36:1985–1991.
98. Wagner A, Mahrholdt H, Holly TA, et al. Contrast-enhanced MRI and routine single photon emission computed tomography (SPECT) perfusion imaging for detection of subendocardial myocardial infarcts: an imaging study. Lancet 2003;361: 374–379.
99. Mahrholdt H, Wagner A, Holly TA, et al. Reproducibility of chronic infarct size measurement by contrast-enhanced magnetic resonance imaging. Circulation 2002;106:2322–2327.
100. Kim RJ, Wu E, Rafael A, et al. The use of contrast-enhanced magnetic resonance imaging to identify reversible myocardial dysfunction. N Engl J Med 2000;16:1445–1453.
101. Schwartzman PR, Srichai MB, Grimm RA, et al. Nonstress delayed-enhancement magnetic resonance imaging of the myocardium predicts improvement of function after revascularization for chronic ischemic heart disease. Am Heart J 2003;146:535–541.
102. Gerber BL, Garot J, Bluemke DA, Wu KC, Lima JA. Accuracy of contrast-enhanced magnetic resonance imaging in predicting improvement of regional myocardial function in patients after acute myocardial infarction. Circulation 2002;106;1083–1089.
103. Perin EC, Silva GV, Sarmento-Leite R, et al. Assessing myocardial viability and infarct transmurality with left ventricular electromechanical mapping in patients with stable coronary artery disease: validation by delayed-enhancement magnetic resonance imaging. Circulation 2002;106:957–961.
104. Kuhl HP, Beek AM, van der Weerdt AP, et al. Myocardial viability in chronic ischemic heart disease: comparison of contrast-enhanced magnetic resonance imaging with (18) F-fluorodeoxyglucose positron emission tomography. J Am Coll Cardiol 2003;41:1341–1348.

105. John AS, Dreyfus GD, Pennell DJ. Images in cardiovascular medicine. Reversible wall thinning in hibernation predicted by cardiovascular magnetic resonance. Circulation 2005;111: e24–25.
106. James O, Kim HW, Weinsaft J, et al. Demonstration and prediction of the potential reversible nature of thinned myocardium by CMR. J Cardiovasc Magn Resonance 2005;7: 69–70(abstr).
107. Bello D, Fieno DS, Kim RJ, et al. Infarct morphology identifies patients with substrate for sustained ventricular tachycardia. J Am Coll Cardiol 2005;45:1104–1108.
108. Wu E, Judd RM, Vargas JD, Klocke FJ, Bonow RO, Kim RJ. Visualization of presence, location, and transmural extent of healed Q-wave and non-Q-wave myocardial infarction. Lancet 2001;357:21–28.
109. Choudhury L, Mahrholdt H, Wagner A, et al. Myocardial scarring in asymptomatic or mildly symptomatic patients with hypertrophic cardiomyopathy. J Am Coll Cardiol 2002;40: 2156–2164.
110. Mood JC, Reed E, Sheppard MA, et al. The histological basis of late gadolinium enhancement cardiovascular magnetic resonance in hypertrophic cardiomyopathy. J Am Coll Cardiol 2004;43:2260–2264.
111. van Dockum WG, ten Cate FJ, ten Berg JM, et al. Myocardial infarction after percutaneous transluminal septal myocardial ablation in hypertrophic obstructive cardiomyopathy: evaluation by contrast-enhanced magnetic resonance imaging. J Am Coll Cardiol 2004;43:27–34.
112. Moon JC, Sachdev B, Elkington AG, et al. Gadolinium enhanced cardiovascular magnetic resonance in Anderson-Fabry disease: evidence for a disease specific abnormality of the myocardial interstitium. Eur Heart J 2003:34:2151–2155.
113. Vignaux O, Dhote R, Duboc D, et al. Clinical significance of myocardial magnetic resonance abnormalities in patients with sarcoidosis: a 1 year follow-up study. Chest 2002;122:1895–1901.
114. Mahrholdt H, Goedecke C, Wagner A, et al. Cardiovascular magnetic resonance assessment of human myocarditis: a comparison to histology and molecular pathology. Circulation 2004;109:1250–1258.
115. Friedrich MG, Strohm O, Schulz-Menger J, et al. Contrast media-enhanced magnetic resonance imaging visualizes myocardial changes in the course of viral myocarditis. Circulation 1998;97:1802–1809.
116. Smedema JP, van Paassen P, van Kroonenburgh MJ, Snoep G, Crijns HJ, Tervaert JW. Cardiac involvement of Churg-Strauss syndrome demonstrated by magnetic resonance imaging. Clin Exp Rheumatol 2004;22:S75–78.
117. Maceira AM, Joshi J, Prasad SK, et al. Cardiovascular magnetic resonance in cardiac amyloidosis. Circulation 2005;111:186–193.
118. McCrohon JA, Moon JC, Prasad SK, et al. Differentiation of heart failure related to dilated cardiomyopathy and coronary artery disease using gadolinium enhanced cardiovascular magnetic resonance. Circulation 2003;108:54–59.
119. Bello D, Shah DJ, Farah GM, et al. Gadolinium cardiovascular magnetic resonance predicts reversible myocardial dysfunction and remodeling in patients with heart failure undergoing beta-blocker therapy. Circulation 2003;108:1945–1953.
120. Kramer CM, Reichek N, Ferrari VA, et al. Regional heterogeneity of function in hypertrophic cardiomyopathy. Circulation 1994;90:186–194.
121. Amano Y, Takayama M, Amano M, Kumazaki T. MRI of cardiac morphology and function after percutaneous transluminal septal myocardial ablation for hypertrophic obstructive cardiomyopathy. AJR 2004;182:523–527.
122. Johnston DL, Rice L, Vick GW 3rd, et al. Assessment of tissue iron overload by nuclear magnetic resonance imaging. Am J Med 1989;87:40–47.
123. Anderson LJ, Holden S, Davis B, et al. Cardiovascular T2* magnetic resonance for the early diagnosis of myocardial iron overload. Eur Heart J 2001;22:2171–2179.
124. Carlson MD, White RD, Trohman RG, et al. Right ventricular outflow tract ventricular tachycardia: detection of previously unrecognized anatomic abnormalities using cine magnetic resonance imaging. J Am Coll Cardiol 1994; 24:720–727.
125. Globits S, Kreiner G, Frank H, et al. Significance of morphological abnormalities detected by MRI in patients undergoing successful ablation of right ventricular outflow tract tachycardia. Circulation 1997;96:2633–2640.
126. Tandri H, Saranathan M, Rodriguez ER, et al. Noninvasive detection of myocardial fibrosis in arrhythmogenic right ventricular cardiomyopathy using delayed-enhancement magnetic resonance imaging. J Am Coll Cardiol 2005;45:98–103.
127. Kupfahl C, Honold M, Meinhardt G, et al. Evaluation of aortic stenosis by cardiovascular magnetic resonance imaging: comparison with established routine clinical techniques. Heart 2004;90:293–301.
128. Caruthers SD, Lin SJ, Brown P, et al. Practical value of cardiac magnetic resonance imaging for clinical quantification of aortic valve stenosis: comparison with echocardiography. Circulation 2003;108:2236–2243.
129. Djavidani B, Debl K, Lenhart M, et al. Planimetry of mitral valve stenosis by magnetic resonance imaging. J Am Coll Cardiol 2005;45:2048–2053.
130. Lin SJ, Brown PA, Watkins MP, et al. Quantification of stenotic mitral valve area with magnetic resonance imaging and comparison with Doppler ultrasound. J Am Coll Cardiol 2004;44:133–137.
131. Higgins CB, Wagner S, Kondo C, Suzuki J, Caputo GR. Evaluation of valvular heart disease with cine gradient echo magnetic resonance imaging. Circulation 1991;84:I198–207.
132. Suzuki J, Caputo GR, Kondo C, Higgins CB. Cine MR imaging of valvular heart disease: display and imaging parameters affect the size of the signal void caused by valvular regurgitation. AJR 1990;155:723–727.
133. Semelka RC, Shoenut JP, Wilson ME, et al. Cardiac masses: signal intensity features on spin-echo, gradient-echo, gadolinium-enhanced spin-echo and TurboFLASH images. J Magn Reson Imaging 1992;2:415–420.
134. Levine RA, Weyman AE, Dinsmore RE, et al. Noninvasive tissue characterization: diagnosis of lipomatous hypertrophy of the atrial septum by nuclear magnetic resonance imaging. J Am Coll Cardiol 1986;7:688–692.
135. Sechtem U, Tscholakoff D, Higgins CB. MRI of the normal pericardium. AJR 1986;147:239–244.
136. Masui T, Finck S, Higgins CB. Constrictive pericarditis and restrictive cardiomyopathy: evaluation with MR imaging. Radiology 1992;182:369–373.
137. Talreja DR, Edwards WD, Danielson GK, et al. Constrictive pericarditis in 26 patients with histologically normal pericardial thickness. Circulation 2003;108:1852–1857.
138. Kojima S, Yamada N, Goto Y. Diagnosis of constrictive pericarditis by tagged cine magnetic resonance imaging [letter]. N Engl J Med 1999;341:373–374.
139. Hundley WG, Li HF, Lange RA, et al. Assessment of left-to-right intracardiac shunting by velocity-encoded, phase-difference magnetic resonance imaging. A comparison with oximetric and indicator dilution techniques. Circulation 1995;91:2955–2960.
140. McConnell MV, Ganz P, Selwyn AP, et al. Identification of anomalous coronary arteries and their anatomic course by

magnetic resonance coronary angiography. Circulation 1995;92: 3158–3162.
141. Post JC, van Rossum AC, Bronzwaer JG, et al. Magnetic resonance angiography of anomalous coronary arteries. A new gold standard for delineating the proximal course? Circulation 1995;92:3163–3171.
142. Vliegen HW, Doornbos J, de Roos A, Jukema JW, Bekedam MA, van der Wall EE. Value of fast gradient echo magnetic resonance angiography as an adjunct to coronary arteriography in detecting and confirming the course of clinically significant coronary artery anomalies. Am J Cardiol 1997;79:773–776.
143. Taylor AM AM, Thorne SA, Rubens MB, et al. Coronary artery imaging in grown-up congenital heart disease: complementary role of MR and x-ray coronary angiography. Circulation 2000; 101:1670–1678.
144. McGee KP, Debbins JP, Boskamp EB, et al. Cardiac magnetic resonance parallel imaging at 3.0 Tesla: technical feasibility and advantages. J Magn Reson Imaging 2004;18:291–297.
145. Sodickson DK, McKenzie CA, Ohliger MA, Yeh EN, Price MD. Recent advances in image reconstruction, coil sensitivity calibration, and coil array design for SMASH and generalized parallel MRI. MAGMA 2002;13:158–163.
146. Botnar RM, Stuber M, Kissinger KV, Kim WY, Spuentrup E, Manning WJ. Non-invasive coronary vessel wall and plaque imaging with magnetic resonance imaging. Circulation 2000; 102:2582–2587.
147. Razavi R, Hill DL, Keevil SF, et al. Cardiac catheterization guided by MRI in children and adults with congenital heart disease. Lancet 2003;362:1877–1882.